Title

Local hydraulics influence habitat selection and swimming behavior in adult California Central Valley Chinook salmon at a large river confluence

Authors

Luis, Sean M

Pasternack, Gregory B

Publication Date

2023-05-01

DOI

10.1016/j.fishres.2023.106634

Fisheries Research 261 (2023) 106634

Contents lists available at ScienceDirect

Fisheries Research

journal homepage: www.elsevier.com/locate/fishres

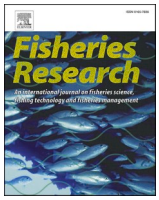

Local hydraulics influence habitat selection and swimming behavior in adult California Central Valley Chinook salmon at a large river confluence

Sean M. Luis *, Gregory B. Pasternack

Department of Land, Air, and Water Resources, University of California at Davis, One Shields Avenue, Davis, CA 95616–8626, USA

ARTICLE INFO

Keywords:
Imaging sonar
Anadromous fish
Homing and straying
River confluence hydraulics
Environmental flow management

ABSTRACT

Migratory habitat selection in adult anadromous salmonids occurs in response to a combination of physical, chemical, and biological cues. Migratory behavioral responses to localized hydraulics are not well understood and hydraulic flow features can be particularly complex at confluence junctions. In some cases, hydraulics may play a partial role in migratory routing, with implications for population structure where wild- and hatchery-origin fish hybridize. This study investigated two questions about such confluences: (1) Can patterns in migratory microhabitat selection or migratory swimming behavior in adult Chinook salmon be attributed to micro-scale hydraulic conditions driven by discharge magnitude and ratio at a confluence? (2) What is the relative influence of selectivity for hydraulic conditions compared to temperature and/or turbidity in micro-scale habitat selection or migratory swimming behavior at a confluence? The fall 2019 migration of California Central Valley Chinook salmon (*Oncorhynchus tshawytscha*) at the confluence of the Feather and Yuba Rivers in northeastern California served as a testbed. Using two dual-frequency identification sonars, 12 monitoring sites representing distinct physical microhabitats upstream of, within, and downstream of the confluence were repeatedly sampled during two four-day flow periods (mean flow ratios between the Feather and Yuba Rivers were 8.66 and 4.02, respectively). Temperature magnitudes and ratios flipped between these sampling periods. We used a multiple regression analysis using the F test for significance and a corrected Akaike information criteria (AICc) analysis to identify predictors of both detection rate (# individuals/m^3/min) and percent occurrence of directed, milling, and backtracking swimming behaviors. A combination of conveyance (m^2/s), temperature, and turbidity was found to perform best in predicting detection rate ($p < 0.001$). No suitable model was found to predict directed behavior. Milling was best predicted by a combination of all hydraulic variables ($p < 0.001$) and although temperature alone was found to best predict backtracking ($p < 0.01$), we identified a candidate model including conveyance and temperature as predictors ($\Delta AICc = 3.66$, $p = 0.02$) which aided in the interpretation of our results. This study provides evidence that channel hydraulics play an active role in the sum of navigation cues that are utilized by migrating adult salmon en route to spawning grounds and should be considered in future investigations of homing and straying patterns in anadromous salmonids.

1. Introduction

Salmon have long been a major focal point in aquatic resource management in the western United States, Canada, and worldwide where such anadromous fish occur, with the goal of maintaining healthy populations for sustainable harvest (Larkin, 1979). The nature of their migration has been studied extensively, as it is a critical facet of their life history strategy (Dittman and Quinn, 1996; Keefer and Caudill, 2014; Putman et al., 2013). In many cases, anadromous fish habitat in regulated rivers experiences altered flow regimes to accommodate agricultural, municipal, and industrial water use throughout the year (Brown and Ford, 2002; Buddendorf et al., 2017; Marchetti and Moyle, 2001; Tsuboi et al., 2010) as well as riverscape narrowing and simplification to accommodate adjacent land use (Jacobson and Galat, 2006).

River confluences can be hydraulically and geomorphologically complex features of regulated fluvial channel networks and represent critical points for successful homing. Understanding of their dynamics (including hydraulic flow features, sediment flux, and channel geometries) has become increasingly more sophisticated since the mid-20th century (Best, 1986; Gualtieri et al., 2017; Miller, 1958; Richards,

* Corresponding author.
E-mail address: smluis@ucdavis.edu (S.M. Luis).

https://doi.org/10.1016/j.fishres.2023.106634
Received 5 August 2022; Received in revised form 18 January 2023; Accepted 19 January 2023
Available online 2 February 2023

1980). For salmon migrating upstream, each confluence that is encountered represents a critical navigational step in a sequence of decisions that must be made between entering the estuary and reaching spawning grounds. In many rivers, the physical, chemical, and biological attributes of migratory habitat at a confluence are dictated by environmental drivers that occur in a spatial hierarchy, from landscape-scale processes down to micro-scale processes.

1.1. Study purpose and scientific questions

This study investigated microhabitat-scale drivers of migratory habitat selection at a regulated river confluence by addressing the following questions: (1) Can patterns in migratory microhabitat selection or migratory swimming behavior in adult Chinook salmon be attributed to micro-scale hydraulic conditions driven by discharge magnitude and ratio at a confluence? (2) What is the relative influence of selectivity for hydraulic conditions compared to temperature and/or turbidity in micro-scale habitat selection or migratory swimming behavior at a confluence? Our study design does not explicitly account for microhabitat selection based on homing fidelity to natal water based on odor cues. It is impossible to disentangle micro-scale preference for temperature and/or turbidity purely based on those physical characteristics from selectivity of natal source water based on chemosensory attraction via olfactory imprinting, or preferences resulting from the water's thermal/optical characteristics at the time of our observation. In our study, we consider the degree to which temperature and turbidity play a role in micro-scale habitat preference as a potential sign of homing fidelity and our results are discussed in that context. The experimental design concept and tested hypotheses are included below in Section 2.2 and summarized in Table 1.

1.2. Conceptual model background

Fig. 1 presents a conceptual model of migratory habitat attributes for adult Pacific salmon that occur within a spatial hierarchy of physical, chemical, and biological processes which directly or indirectly drive habitat selection at river confluences. An expanded literature review and synthesis supporting the conceptual model is included in Section 1 of the appendix. It is important to consider the potential roles of landscape-, reach-, and micro-scale phenomena that affect fish migratory decision-making and/or behavior instincts when a fish arrives at a confluence.

1.2.1. Landscape-scale habitat attributes

Landscape-scale hydrologic and sediment supply regimes act as top-down controls on local flow magnitude, frequency, duration, timing, and rate of change, including interannual variation of these attributes (Edwards et al., 2015). River discharge at a catchment or reach scale has been used to partially explain the timing of population-level adult salmon migratory movements with implications for flow management in the context of accommodating or facilitating migration (Anderson and Beer, 2009; Dahl et al., 2004; Peterson et al., 2017). In catchments with regulated rivers, many dam operation schedules are partially planned to control downstream discharges (Acreman et al., 2009; Bradford et al., 2011; Gendaszek et al., 2018; Saltveit et al., 2019), as well as temperatures (Ahmad and Hossain, 2020; Nichols et al., 2014; Rheinheimer et al., 2015) to accommodate specific salmonid lifecycle stages and their habitat requirements. Along with climate and precipitation patterns, regional orogeny, epeirogeny, and lithology act as major drivers of sediment transport dynamics, drainage pattern, and spatial distribution of channel types (Dietrich et al., 2003; Howard et al., 1994; Massong and Montgomery, 2000; Sklar and Dietrich, 2001). These landscape-scale processes ultimately determine the amount and type of habitat available to a salmon population by dictating the spatial extent and distribution of alluvial channel forms (Church, 2006).

Hatchery production facilities can induce population-level effects when juveniles are reared to the parr/smolt stage and released off site to avoid mortality associated with downstream migration (Huber and Carlson, 2015; Murdoch et al., 2009). This is thought to result in increased rates of straying in adults due to the interruption of olfactory imprinting at earlier life stages (Jonsson et al., 2003; Keefer and Caudill, 2014; Sturrock et al., 2019). In addition to hatchery release practices, some pollutants are known to disrupt olfaction via toxicity to the olfactory physiology of salmonids by multiple biochemical pathways (Tierney et al., 2010). Many salmon populations occur in regions that experience extensive agricultural land use and large-scale application of pesticide compounds that enter waterways via agricultural runoff.

1.2.2. Reach-scale habitat attributes

Except for some Alaskan chum salmon (*O. keta*) runs (known to occasionally spawn in intertidal areas of river mouths, see Johnson et al., 1997), most adult Pacific salmon undergo some degree of upstream migration into a catchment, encountering a sequence of tributary confluences. The distance travelled along a migration route can vary within and among species (Quinn, 2018). The types of riverine habitats occupied by Pacific salmon species throughout their range are highly variable as well. As they progress through their upstream migration, salmon experience variation in both channel discharge, geometry, and local features, such as deposited wood, boulders, bank outcrops, man-made structures, etc. This dynamic combination of flow and channel shape dictates the hydraulic conditions that each individual experiences. Hydraulic connectivity and passage capability at knickpoints are major factors that determine how far into a channel network an individual fish can swim. Confluences within a catchment can be important drivers of reach-scale geomorphic features and resultant physical migratory habitat structure (Blettler and Amsler, 2016; Penna et al., 2018). In a review of "confluence effects" in drainage networks, Benda et al. (2004) found a correlation between the ratio of tributary and mainstem drainage area and the probability of confluence effects occurring (meaning the formation of fluvial landforms associated with confluences such as fans, bars, and terraces). In certain cases, sediment aggradation at channel confluences may interrupt downstream sediment supply, disrupting alluvial processes that facilitate physical habitat heterogeneity downstream of the confluence. The extent to which this occurs within a basin is largely driven by drainage area and stream network length (Rice, 2017).

Because acute injury to olfactory organs has been demonstrated in the presence of certain pesticide compounds (Tierney et al., 2008), it is possible that non-point source contamination may have some influence in migratory routing at confluences above a concentration threshold for acute toxicity. Point source contamination may also have reach-scale

Table 1
Hypotheses and test methods used in this study. Predictor variables a-g are each tested as a separate hypothesis in the analysis. Directed, milling, and backtracking behaviors are defined in Section 2.3.3.

Hypothesis		
H_1: Detection rate* correlates with…	a	Velocity magnitude
	b	Depth
	c	Conveyance
	d	Froude number
	e	Temperature
	f	Turbidity
	g	Multiple Predictors
Percent of _____ swimming behavior correlates with…	a	Velocity magnitude
H_2: Directed* *	b	Depth
H_3: Milling* *	c	Conveyance
H_4: Backtracking* *	d	Froude number
	e	Temperature
	f	Turbidity
	g	Multiple Predictors

* Nonlinear (exponential) regression * *Linear regression. Hypothesis testing utilizes the F test for multiple regression coefficients being non-zero (95% confidence).

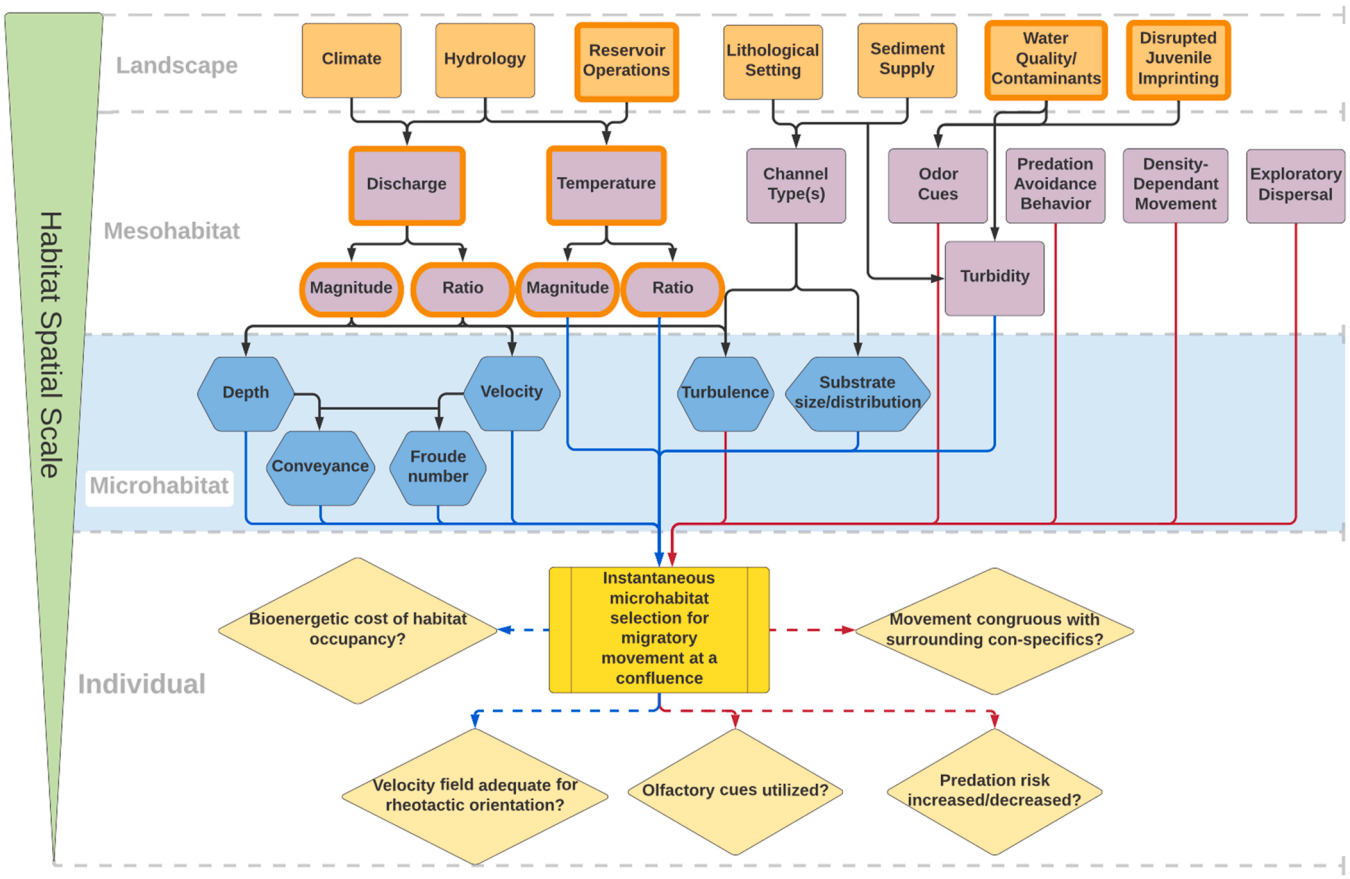

Fig. 1. Conceptual model diagram summarizing physical and biological drivers involved in multi-scale habitat selection by anadromous migrating adult salmonids at river confluences. Black lines indicate indirect drivers of habitat selection. The area shaded in blue includes microhabitat attributes that are investigated in this study (with the exception of turbulence). Blue lines indicate direct drivers that are quantified and analyzed in this study, while red lines indicate direct drivers that are not measured. Items outlined in orange indicate physical and biological drivers that are actively managed, either partially or fully. Yellow diamonds describe the physiological and behavioral implications for a given movement by an individual. Dotted blue arrows are ecological implications that could be accounted for using the results of this study, and red dotted lines cannot.

impacts to adult salmon migratory habitat via contaminant spills, poor pesticide management practices, or concentrated discharge of agricultural runoff during dry periods (Holvoet et al., 2007; McKnight et al., 2015).

It is also important to note that some amount of straying occurs naturally across Pacific salmon species. Exploratory dispersal as an innate behavior appears to be an expression of the portfolio effect in their life history strategy and in some cases may be related to thermoregulation (Goniea et al., 2006, High et al., 2006, Peterson et al., 2016, Schindler et al., 2010, Keefer et al., 2018). Beyond biological cues at the individual level, recent evidence has demonstrated density-dependent movement of spawning cohorts (Berdahl et al., 2017, 2016). Further investigation is needed before a density threshold for aggregated group movement can be identified across salmonid taxa. Finally, little is known about predator avoidance dynamics in migrating adult salmon, though it is thought to be most important on or near spawning grounds (Quinn, 2018; Quinn et al., 2001).

1.2.3. *Micro-scale habitat attributes*

Channel discharge, geometry, and sediment composition act together to produce micro-scale physical habitat conditions commonly referred to as “microhabitats”. The microhabitat spatial scale is defined by Baldes and Vincent (1969) as “the physical conditions immediately surrounding an animal at a given time and place”. This spatial scale has been utilized in investigations into life stage-specific habitat requirements (Carnie et al., 2016; Moir and Pasternack, 2010; Nielsen, 1992; Shirvell, 1994), restoration design and planning applications (Brown and Pasternack, 2009; Fangue et al., 2021; Favrot et al., 2018), and evaluation of passage infrastructure (Li et al., 2021; Nestler et al., 2008; Weber et al., 2006). To date, the influence of confluence hydraulics on species-specific microhabitat distribution in space and time has not yet been studied.

2. Materials and methods

2.1. *Study area and management context*

The Feather and Yuba River catchments lie adjacent in the northeastern area of the California Central Valley (Fig. 2). Both experienced intensive hydraulic gold mining activity during the 19th century. Differences in early river engineering approaches resulted in contrasting channel evolution processes, particularly with regard to levee width (James et al., 2009). The Yuba drainage area is 3480 km^2 and the lower Yuba River (LYR) is a 37.1 km segment between Englebright Dam to the confluence with the lower Feather River (LFR). It is dominated by gravel/cobble substrate, transitioning to a sand-dominant channel at the confluence. The Feather drainage area is 16,050 km^2 and the LFR extends 117 km from Oroville Dam to its confluence with the Sacramento River. The LFR is dominated by finer sediment and has experienced significant channel avulsion. The Oroville spillway collapse in 2017 resulted in the rapid mobilization of approximately 1 million metric tons of debris that was deposited in adjacent floodplain areas (Nalin and Kotulla, 2018). The LFR is also heavily influenced by Thermalito Afterbay, a series of hydraulically connected shallow reservoirs adjacent

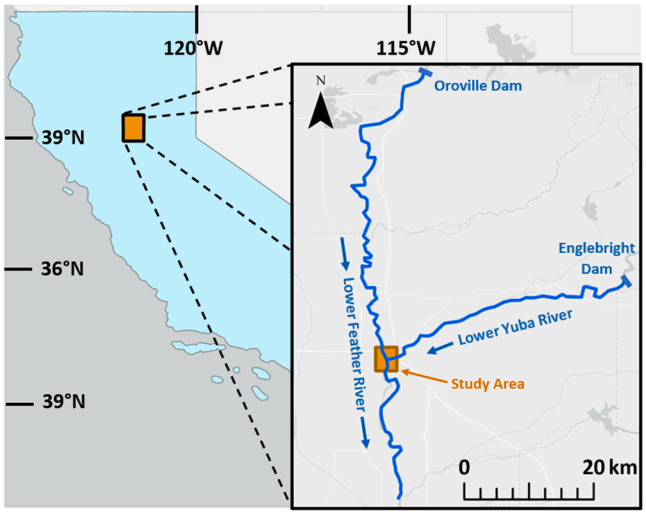

Fig. 2. Location of the study area. The state of California is shaded in blue in the main panel. The inset identifies the lower Feather River, lower Yuba River, and the dams that create total fish passage barriers upstream of the study area. Blue arrows indicate flow direction. Base map image sources: ESRI, HERE, Garmin, FAO, NOAA, USGS, © OpenStreetMap contributors, and the GIS user community.

to the main channel that result in increased water temperatures. Both rivers are regulated and experience annual flow regimes that are altered from historical conditions, though the LYR has a relatively natural flood regime (Gervasi et al., 2021).

The location of the study area is the immediate confluence of the LFR and LYR. Specifically, it includes approximately 1.42 km of the LFR and 0.85 km of the LYR upstream of the confluence and 1.13 km of the LFR downstream of the confluence (Fig. 3). The study area is dominated by sand-sized substrate with small patches of coarser material in fast-moving riffles (see Table A.1 for grain size distribution by sample site in the appendix). Topographic surveys and aerial imagery indicate that the study area is subject to significant interannual changes in channel geometry due to mobilization of fine sediment during winter high flow periods. In-stream wood is present along the banks and can be submerged; more wood occurs in the LYR, because the west bank of the LFR has a sandy levee and that bank is subject to maintenance and clearance.

The Feather River Fish Hatchery is located at the base of Oroville Dam and is one of the largest production facilities for fall-run Chinook in the Central Valley. In 2019, spring- and fall-run Chinook produced by Feather River Fish Hatchery accounted for 43.6% of adult hatchery-origin Chinook collected in the Sacramento and San Joaquin basins during the fall-run escapement period (CDFW, 2021). The hatchery is located ~ 61.9 RKM upstream of the study site. In 2019 (the year that our field surveys took place), 27,103 Chinook salmon returned to the hatchery with 51,967 in-river returns, totaling 79,070 fish (CDFW, 2022). The LYR has no hatchery production facility and extant naturally spawning populations of spring- and fall-run Chinook persist. In 2019, the LYR experienced 3446 in-river returns (CDFW, 2022).

The Yuba Accord River Management Team (YARMT) found that discharge magnitudes differing between the two rivers appear to influence navigational choice at the LFR-LYR confluence (YARMT, 2013). Correlative patterns have emerged in the two rivers between escapement rates for spring- and fall-run Chinook and discrepancies in the magnitude of flow and temperature between the rivers in certain years. Monitoring data show that in years with higher discharge and lower temperature in the LYR relative to the LFR, high rates of straying of Feather-origin fish can be seen in the LYR.

In surveys conducted from 2004 to 2011, YARMT counted the number of Feather-hatchery origin fish passing a low-head dam on the LYR and, using a fitted logistic model, found that 72% of the variation in

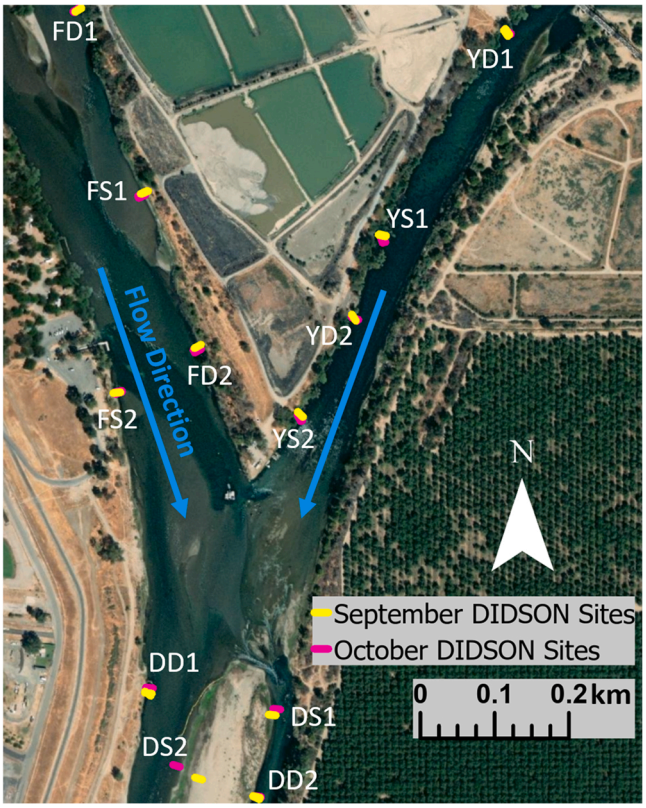

Fig. 3. DIDSON deployment sites with centerlines indicating orientation (colors indicate sampling period). Sites are classified as being in the Feather, Yuba, or downstream zones (F, Y, and D), and whether it was a deep or shallow site (D or S, two in each zone). Base map image sources: ESRI, Maxar, Earthstar Graphics, and the GIS user community.

the proportion of hatchery- and wild-origin adults entering the LYR could be attributed to the ratio of discharge magnitude between the two rivers and the ratio of water temperature between the two rivers. As a result, the National Marine Fisheries Service's California Central Valley Salmonid Recovery Plan includes a recovery action to "evaluate whether salmonid straying between the Feather and Yuba rivers can be minimized through flow management" (NMFS 2014). It may be necessary to co-manage the LFR and LYR to a degree to address this.

Based on the results of YARMT's monitoring efforts and the extent to which migratory behavioral cues in adult salmon are characterized in the literature, there is a clear need to go beyond simple empirical correlations to investigate potential mechanisms of straying behavior at the LFR/LYR confluence driven by local physical processes that convert general drivers like discharge and temperature into sensory experiences fish use to make decisions or respond to instinctually. Beyond the direct management implications for hatchery-origin fish occupying these watersheds, such an investigation would aid in filling a critical knowledge gap in the migratory physiology and behavior of anadromous salmonids.

It may be that the cue is simply magnitude of discharge, but how can that be possible mechanistically? Specifically, how can a fish experience an instantaneous total volume of water passing a cross-section that is ~ 300 times wider than their body length? That is unlikely. Instead, it is most likely that discharge is a distal "black box" governing variable inducing the ecohydraulic mechanism by which a proximal physical template is presented to fish for their behavioral response. The risk of relying on empirical analysis of only one governing variable without investigating underlying mechanisms is that important, yet unaccounted for other governing variables (e.g. topography, substrate, vegetation, stream wood, etc.) could change independently of managers tuning flow releases, resulting in a poor or ambiguous outcome from controlled

actions. Further, there remains ~ 30% of the behavioral decisions that are not explained by the empirical analysis, and that constitutes a sizable population-level effect that needs to be understood (YARMT, 2013).

2.2. Experimental design concept

As shown conceptually in Fig. 1, this study investigated drivers of migratory microhabitat selection at a regulated river confluence. Depths and velocities throughout the study site experienced top-down control by discharge magnitude and ratio (referred to as "discharge condition") between the LFR and LYR. Discharge condition changed considerably between September and October sampling periods in 2019. Fixed DIDSON sampling sites were selected to capture the broadest possible range of depth and velocity magnitude values to identify one or both of those attributes as drivers of selection ("deep" and "shallow" site type designations, see Figs. 3 and 4). The study area was divided into three zones that experienced different overall velocity conditions depending on their orientation to the confluence. The three zones include the LYR portion upstream of the confluence, referred to as the "Yuba" zone; the LFR portion upstream of the confluence, referred to as the "Feather" zone; and the LFR portion downstream of the confluence, referred to as the "downstream" zone.

Detection rate data from our DIDSON surveys were fit to a set of multiple non-linear regression models to investigate the strength of four hydraulic variables (velocity magnitude; depth; Froude number, a dimensionless quantity that represents the ratio of inertial forces to gravitational forces; and conveyance, a representation of the flow per unit-width that an individual fish experiences at a given point along their migratory pathway) as well as temperature and turbidity, as predictors of micro-scale habitat selection. The sediment grain size distribution within the study area is dominated by sand and therefore would not serve as a useful predictor of habitat selection (see Table A.1 in the appendix). The candidate models as well as the regression function (exponential) were selected based on preliminary exploration of the detection rate data. Additionally, we analyzed migratory swimming behavior type by measuring a combination of rheotactic orientation and progress over ground. This yielded a Eularian-based indicator of upstream migration, and it cannot be used to truly characterize Lagrangian-based movement (Doyle and Ensign, 2009; Willis, 2011). Swimming behavior types were designated as "directed", "milling", and "backtracking" as detailed below. The same set of multiple regression models was used to predict percent occurrence of each of these swimming behaviors, but these models were instead fit using a linear regression type. An Akaike information criteria analysis corrected for small sample sizes (AICc) was used to score and rank the suitability of the models for predicting each response variable. F tests for statistical significance in each regression fit served as a test metric for our stated hypotheses in Table 1.

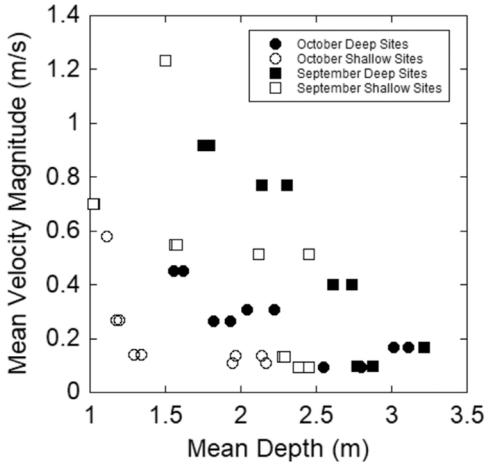

Fig. 4. Mean depths are plotted against mean velocity magnitude for each DIDSON deployment site in both sampling periods. Some overlap occurs between "deep" and "shallow" sites as they were selected based on relative depths within each zone of the sampling scheme.

2.3. DIDSON surveys

2.3.1. DIDSON sonar

The potential utility of dual-frequency identification sonars (DIDSON) technology for biological research applications has been noted for settings in which optical underwater imaging equipment may be limited by light, turbidity, or suspended particulate matter (Belcher et al., 2002, 2001). Moursund et al. (2003) assessed the feasibility of DIDSON technology in fisheries research applications. Since then, it has been used to monitor salmon passage rates in Alaska (Faulkner and Maxwell, 2009; Maxwell and Gove, 2004, 2007) and fish behavioral responses to passage infrastructure in Australia (Baumgartner et al., 2006). It has also been used for steelhead (*Oncorhynchus mykiss*) population assessments in coastal California watersheds (Pipal et al., 2012) and green sturgeon (*Acipenser medirostris*) abundance estimates in the Sacramento River (Mora et al., 2015).

To assess fine-scale hydraulic habitat selection at the LFR/LYR confluence, two DIDSON systems were used to observe migratory behavior and quantify rates of habitat selection within the immediate area of the confluence. A DIDSON system (Sound Metrics Corp.) features a multibeam transducer that emits 48 beams spaced 0.4° apart when operated at the 1.0 MHz frequency and 96 beams spaced 0.3 ° apart with two operating at the 1.8 MHz frequency. The beams are emitted through an "acoustic lens" that can shape the resultant sonar images to focus on a particular field of view.

2.3.2. DIDSON sampling scheme

Migratory behavioral observations via DIDSON occurred over the course of two 4-day sampling periods in 2019, representing markedly different discharge conditions at the confluence due to the scheduled decrease in Feather River flows for salmon spawning in mid-October (CDWR and CDFG, 1983; NMFS, 2016). The first period occurred from September 23–26 and the second from October 22–25. During the first sampling period, mean discharges on the LFR and LYR were ~ 213 and 24 m^3/s, respectively. During the second period, discharges on the LFR and LYR were ~ 68 and 17 m^3/s, respectively (CDWR 2021). Discharge decreased because of a scheduled annual flow decrease in the LFR to prevent anadromous fish from spawning in overbank areas that may be dewatered (CDWR and CDFG 1986, NMFS, 2016). LYR discharge also decreased, but not by as much, yielding a lower flow ratio. Scheduled facility maintenance typically yields the lowest discharge out of Englebright Dam in September. However, actual released discharge may be higher than scheduled depending on carryover storage, natural autumn runoff, and water demand by Yuba County farmers. Further, the timing of LYR flow reduction is earlier than it is for the LFR, so the main effect on the flow ratio in late September is driven by the LFR. Independently of releases, minimum flow requirements on the LYR close to the confluence with the LFR are identical for September and October regardless of water year type used to define the operational schedule in the Yuba Accord. Therefore, the primary control on discharge ratios at the confluence is LFR flow operations.

We established four DIDSON deployment sites in three zones, in both the LFR ("Feather" sites) and LYR ("Yuba" sites) upstream of the confluence and an additional four in the LFR downstream of the confluence ("Downstream" sites). Each of these three zones included two "deep" and two "shallow" sites, relative to surrounding channel topography. Site selection was somewhat limited by availability of shoreside area for equipment set up and deployments were limited to normal daylight working hours due to logistical constraints and safety concerns. The goal of the sampling scheme was to capture a range of

depth and velocity that were representative of the study area. These sites and their physical attributes are shown in Fig. 4 and summarized in detail in Table A.2 in the appendix.

All 12 DIDSON deployment sites were sampled twice for a duration between 30 and 60 min within each 4-day period at a fixed range of 10 m. Deployment locations during the second sampling period were moved laterally into the wetted channel to accommodate the stage drop. DIDSON transducers were suspended in stationary PVC cages and both sonar and laptop equipment were powered by 12 v deep cycle marine batteries. For all deployments, a handheld Trimble GeoHX GeoExplorer 2008 Series GPS was used to obtain a position fix for the transducer. A handheld compass and angle measuring device were used to obtain the compass heading and downward (pitch) angle orientation of the transducer. Roll angle was minimized to the maximum extent possible. From the digital elevation model (DEM, described below) and the transducer position information for each deployment, volumes sampled were estimated using a geometric solution scheme (details included in Figure A.1 in the appendix). Sampling bias was not found to influence detection rates with regards to volume sampled, deployment time, deployment duration, or mean body length estimate. This is discussed further in Section 2.5 of the appendix. A thorough discussion of the species identification criteria used in this study is included in Section 2.6 of the appendix with body length estimates being the primary metric used to identify adult Chinook salmon in the DIDSON footage.

2.3.3. Detection rates and swimming behavior

Individual DIDSON files (recorded at 8 frames per second) were reviewed manually at 30 frames per second and processed to obtain migratory behavioral data for adult Chinook salmon. Footage at the beginning and end of each file that contained camera movement was discarded. Each time a fish entered the field of view that fit the species identification criteria, it was measured three times using the DIDSON software's measuring tool to obtain a mean body length. The time of entry and exit was recorded as well as it's rheotactic orientation to the flow. Detection rates for each deployment were calculated by summing the number of individual detections and dividing those by the minutes of footage analyzed multiplied by the volume of water sampled by the DIDSON:

$$D = \frac{\sum (I)}{t_A V} \tag{1}$$

where D is the detection rate, I is the number of individual detections per site, t_A is the time of footage analyzed in minutes, and V is the total volume of water sampled by the DIDSON in m^3.

Migratory swimming behavior was identified for each detection based on both rheotactic orientation to the flow and movement over ground at each DIDSON site. Fish that showed positive rheotaxis (body oriented against the flow direction) were said to exhibit either "directed" movement if their path of travel over ground was only upstream, or "milling" if their path over ground included both upstream and downstream movement. Fish were said to be "backtracking" if they exhibited negative rheotaxis (body oriented with the flow direction).

2.3.4. Bathymetric mapping

A DEM was constructed using topo-bathymetric point data from GPS and echosounding. Bathymetric mapping of the wetted channel occurred several weeks prior to the behavioral surveys in August 2019 using a Hydrolite single beam echosounder (minimum depth of 0.3 m; depth accuracy of 1 cm; sampling frequency of 200 Hz; Seafloor Systems, Inc.) in sync with a Trimble R8 real-time kinematic GPS (horizontal and vertical accuracies of ~ 1 and 2 cm, respectively) receiving corrections over the internet from a regional base station network on the fly at 1 Hz. Several cross-sectional transects were mapped at each DIDSON deployment site. Additional cross-sectional transects were mapped approximately one channel width apart as well as 8–12 longitudinal transects that spanned the length of each zone in the study area. Bare-Earth topography was collected in January 2020 on an island at the confluence junction using the Trimble R8.

ESRI ArcGIS software was used to process survey data and produce a DEM. Erroneous survey data points were manually identified and removed. Additional augmented points were added along known contours from the field work to smooth any artifacts in the digital terrain that resulted from topographic data gaps. A triangulated irregular network was produced from the point data and then this was converted into a 0.3-m resolution raster. Raster resolution was selected based on the overall density of topographic data points and especially considering point density in the vicinity of DIDSON deployments.

2.4. Hydraulic data

On September 19th and 20th, one week prior to the first behavioral observation period, and again on October 30th, one week following the second behavioral observation period, velocity measurements were taken at each of the DIDSON deployment sites using a boat-mounted Sontek M9 acoustic doppler current profiler. At each DIDSON cross section, six lateral velocity transects were performed, capturing column-wise velocity measurements in succession across the channel. Transects extended the full width of the wetted channel for each sampling period. Mean velocity magnitude values were computed for each column over a 1-second time step and positions were recorded using a Sontek DGPS antenna. The points that were taken from these data in GIS to represent each DIDSON site occurred adjacent to the centerline of the DIDSON beams, within the lateral length of the DIDSON beams in the up or downstream direction. Points included in this search area were then averaged to generate one mean velocity magnitude value for each DIDSON site. During the October sampling period, two of the DIDSON sites were not accessible by boat (DS1 and DD2) and no ADCP data were collected. As a result, those DIDSON deployments were discarded and excluded from our analysis. Mean depth estimates for each DIDSON site were estimated based on the 10-m-long centerline of the DIDSON field of view, using bed elevation measurements from the DEM raster along the centerline at 0.3 m intervals and assuming a uniform transducer submergence depth of 0.9 m at all sites.

Froude number is a dimensionless quantity that represents the ratio of inertial forces to gravitational forces and has been used by others to assess habitat suitability for salmonids (Ayllón et al., 2009; Lamouroux and Souchon, 2002; Persinger et al., 2011):

$$\underline{Fr} = \frac{\underline{u}}{\sqrt{g * \underline{d}}} \tag{2}$$

where u is the mean velocity magnitude at each site in m/s, g is the gravitational acceleration constant in m/s^2, and d is the mean depth at each site in m. Conveyance is defined as follows:

$$\underline{C} = \underline{u} * \underline{d} \tag{3}$$

where u is mean velocity magnitude in m/s and d is mean depth in m. C results in units of m^2/s. Conceptually, it is the discharge per unit width of the wetted channel. It is a representation of the flow that an individual fish experiences at a given point along their migratory pathway. This metric has been used in similar applications for assessing salmonid habitat suitability (Kammel et al., 2016; Moniz et al., 2019).

2.5. Hydraulic model

The overall hydraulic conditions that were available to fish at the study site could not be directly measured for a comparison against those conditions where fish were located, so they were estimated using the two-dimensional (2D) hydrodynamic model TUFLOW HPC (Build 2018–03-AE; BMT Commercial Australia Pty Ltd). The model simulated steady state hydraulics through the study area for the regulated, steady

mean daily discharges that occurred during each sampling period. Gridded model solutions for depth and velocity magnitude were generated with a computational square cell size of 3 m x 3 m. Velocity magnitude validation found model predictions to be a good fit to the data on the basis of an r^2 value of 0.76, which is quite high compared to the literature using 2D hydrodynamic models. Details on the hydrodynamic models including inputs, topographic data, parameters, and validation can be found in Table A.3 of the appendix.

2.6. Temperature and turbidity monitoring

Temperature and turbidity were monitored at fixed sampling locations throughout the 2019 field campaign to represent both discharge conditions (Fig. 5). All but two DIDSON sites had a corresponding temperature/turbidity site, the remaining two were assigned averaged temperature/turbidity values from sites directly up- and down-stream. Three HOBO Water Temperature Pro V2 data loggers (Onset Computer Corp.) were permanently installed at depths of ~ 1 m at each boundary of the project area (Fig. 5) to generate a continuous temperature time series during the two sampling periods (Fig. 6). The purpose of the fixed loggers was to account for any changes in temperature within each 4-day DIDSON sampling period. Fixed HOBO loggers recorded water temperatures (± 0.2 °C) at 30-minute intervals. To avoid dewatering during the Feather discharge decrease and stage drop between DIDSON sampling periods, the fixed loggers were vertically repositioned to achieve > 0.5 m depth submersion for the October

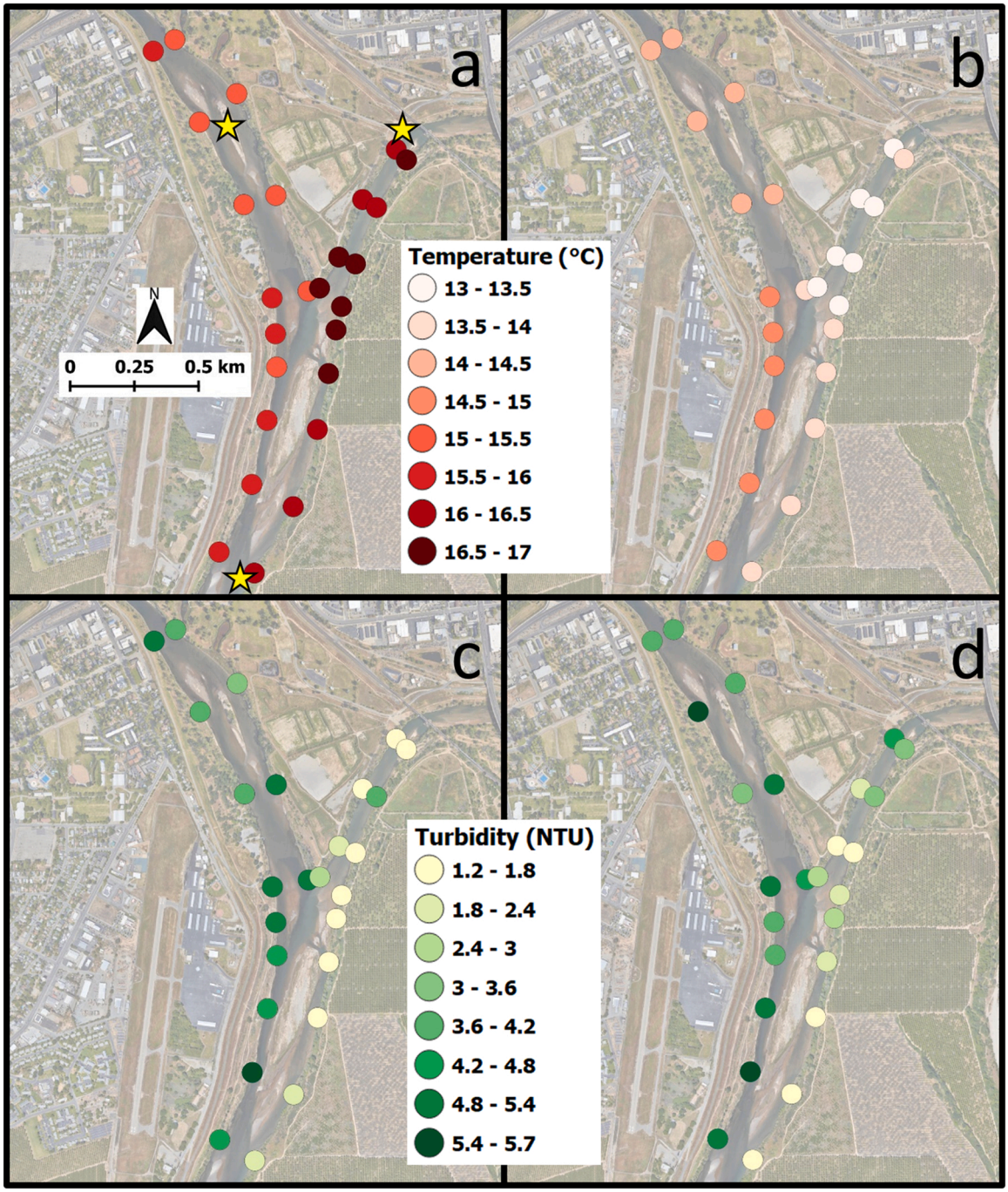

Fig. 5. Locations and results of hand-held surface temperature and turbidity measurements for September (a,c) and October (b,d) sampling periods. The yellow stars indicate the locations of the fixed temperature loggers. Base map image is from Google Earth.

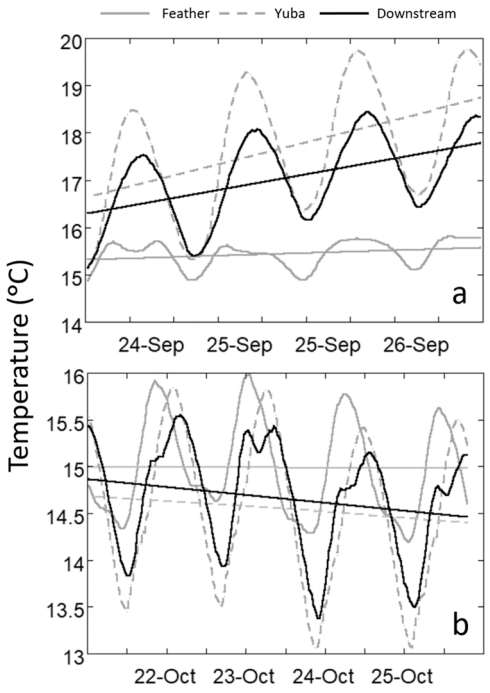

Fig. 6. Temperature time series from each of the three fixed HOBO data loggers during both the September (panel a) and October (panel b) DIDSON sampling periods in 2019. In the September plot, slopes and intercepts for the Feather, Yuba, and downstream temperature time series trendlines are 0.0016, 0.0124, 0.0088, and 15.32, 16.65, 16.30, respectively. In the October plot, slopes and intercepts for the Feather, Yuba, and downstream temperature time series trendlines are − 0.0001, − 0.0014, − 0.0021 and 15.01, 14.68, 14.87, respectively.

period.

Temperature data from the loggers were supplemented with handheld measurements taken at fixed sampling locations (Fig. 5) before and after each DIDSON sampling period (samples taken September 20th and 27th and October 18th and 26th). A resistance temperature detector thermometer (± 0.3 °C) with a general immersion probe (Tegam Inc.) was used to take surface measurements at each station. A third HOBO logger attached to a pole was used to take temperature measurements at 1 m depth or at the bottom (if shallower than 1 m) at each station. Surface and submerged temperatures were compared to determine if vertical temperature stratification occurred at any point in the site.

A 2100Q Portable Turbidimeter (± 2% of reading; HACH Company) was used to measure turbidity in nephelometric turbidity units (NTUs) at each of the handheld temperature monitoring stations. Three measurements were taken at each station and averaged. Sampling vials were rinsed with distilled water between each measurement and the instrument was calibrated at the start of each sampling day in accordance with manufacturer guidance.

2.7. Data analysis

A key question to address was whether the locations where fish were present were distinguishable from the overall river confluence conditions. Mann-Whitney U tests are a typical approach to answering this question, so they were performed using the base R package *stats* (MacFarland and Yates, 2016; R Core Team, 2022b) to test (at 95% confidence) for differences in means between both velocity magnitude and depth values associated with each DIDSON detection, and randomly sampled modeled values from outside of the DIDSON sample sites, representing conditions present within the study area at the time of observation. This was performed across all detections, as well as individually for the September and October sampling periods, which is two variables times three time intervals yielding six total tests. The number of randomly sampled modeled values for velocity magnitude and depth used in each comparison was equal to the number of detections associated with that comparison (228 for all detections, 188 for the September comparison, and 40 for the October comparison).

Per hypotheses H_1 in Table 1, nonlinear regression was used to test for correlation between detection rate and four micro-scale hydraulic variables ($H_{1a\text{-}d}$), temperature (H_{1e}), turbidity ($H_{1\,f}$), and several combinations of these predictors that were assembled based on preliminary exploration of our data ($H_{1\,g}$). Data were fit to exponential functions using a nonlinear ordinary least squares approach (Motulsky and Ransnas, 1987; Ritz and Streibig, 2008) via the base R function '*lm*' and using the F statistic at 95% confidence to test whether at least one regression coefficient was non-zero (Olive, 2017; R Core Team, 2022a). The same R function was used to test the same predictor variables and candidate models on our swimming behavior data using linear regressions. Percent occurrence of each behavior type was the response variable in these models (testing H_2: % directed, H_3: % milling, and H_4: % backtracking). In addition to the F test for significance, the coefficient of determination (r^2) indicated the amount of variance explained by each model. The list of candidate models that was generated to test our stated hypotheses and our rationale for each are included in Table A.4. in the appendix in accordance with best practices for information-theoretic data analysis described by Anderson and Burnham (2002). A preliminary examination of our DIDSON detection data helped inform this list by eliminating model candidates that would likely have poor explanatory power.

We utilized Akaike information criteria corrected for small sample sizes (AICc) to identify the most appropriate model for predicting each response variable using the R package *AICcmodavg* (Cavanaugh and Neath, 2019; Mazerolle, 2020). AICc produces a ranked list of candidate models with the most appropriate (lowest AICc score) striking a balance between having the best fit to the data while also having the fewest predictive parameters used to achieve that fit. A ΔAICc for a given model that is < 2 indicates substantial empirical support for that model whereas values > 10 offer essentially none (Cavanaugh and Neath, 2019). Finally, the AICc weight of support (w) can be interpreted as the probability that a given model is the most appropriate of the list under the AICc. It is computed by normalizing the likelihoods of candidate models in a list so that w values sum to 1. The value of w for model i is expressed as:

$$w_i = \frac{e^{-0.5\Delta \mathrm{AICc}_i}}{\sum_{i=1}^{M} e^{-0.5\Delta \mathrm{AICc}_i}} \quad (4)$$

where M is the number of candidate models in the list (Portet, 2020). Finally, the R package *car* (Fox et al., 2022) was used to generate added variable plots (AVP) for the top AICc-ranked model for each response variable. Each panel in an AVP includes a single parameter from the model plotted against the response variable while holding all other parameters constant and a line is fit to the data (Johnson and McCulloch, 1987). The AVP is a useful diagnostic tool in regression applications as the degree of departure of the line from horizontal indicates the relative strength of its predictive influence in the model.

3. Results

Overall, DIDSON surveys yielded a total of 228 adult Chinook salmon detections (Table 2). Considerably more occurred during the September sampling period (188) than the October period (40). Feather sites upstream of the confluence had the most detections across both sampling periods (163), while the Yuba sites had the least (18); Downstream sites were in between (47). Finally, deep sites showed more detections across both periods (170) than shallow sites (58). Swimming behaviors among all detections occurred as follows: directed (135), milling (39), and backtracking (54). Details on detections per swimming behavior as a

Table 2
Total number of detections by sampling period, study area zone, and site type. Also included are total detections by swimming behavior type as a function of sampling period, study area zone, and site type. This information also serves as the contingency tables for the Chi-squared analysis performed in this study.

	Detection Summary						Swimming Behavior Summary		
	Total	Sampling Period		Sampling Zone					
		September	October	Feather	Yuba	Downstream	Directed	Milling	Backtracking
Overall	228						135	39	54
September Period	188						120	25	43
October Period	40						15	14	11
Feather Zone	163	147	16				105	16	42
Yuba Zone	18	6	12				10	1	7
Downstream Zone	47	35	12				20	22	5
Deep Sites	170	151	19	134	5	31	107	16	47
Shallow Sites	58	37	21	29	13	16	28	23	7

function of sampling period, zone, and deployment site type (deep vs. shallow) are included in Table 2. Table A.2 in the appendix includes detection rates for each DIDSON deployment (ranging from 0.001 to 1.87 #/min/m^3 for sample sites that included ≥ 1 salmon detection) as well as their corresponding habitat attributes. It is important to note that one deployment (the second deployment at site FD2 in September) had an exceptionally high detection rate compared to all other deployments and accounted for 48% of all fish detections. We chose not to exclude this deployment as an outlier because it shared similar hydraulic site attributes as other deployment sites with high detection rates. The implications of including this site in our analysis are discussed in detail below.

Mean surface temperature and turbidity values for the hand-held surveys showed the LFR to be more turbid in both sampling periods with a notable shift in cooler temperatures between periods from the LFR to the LYR (Fig. 5). Vertical temperature differences were measured to demonstrate that they were negligible and did not introduce potential bias based on vertical swimming positions of fish. In September, vertical temperature differences ranged from − 0.54–0.77 °C with a mean difference of 0.069 °C and median difference of 0.065 °C. In October, vertical temperature differences ranged from − 0.18–1.30 °C with a mean difference of 0.42 °C and median difference of 0.39 °C. Fig. 6 shows 30-min temperature measurements taken by the fixed HOBO data loggers. Linear curves fit to the temperature timeseries indicate slight increases throughout the DIDSON sampling period in September for the Feather, Yuba, and Downstream loggers. In October, the timeseries show slight decreases in temperature throughout the DIDSON sampling period.

Modeled velocity magnitude values throughout the study area ranged from 0 to 1.22 m/s in September and 0 – 1.75 m/s in October. Modeled depth values throughout the study area ranged from < 0.01 – 5.66 m in September and < 0.01 – 4.90 m in October. Percent occurrences of binned, modeled depth and velocity magnitude values throughout the study area are summarized in Table 3, where the greatest percent occurrences for both modeled depth and modeled velocity decrease from September to October.

Comparisons of means and standard deviations between observed and modeled available hydraulics revealed that differences in depths were greater than differences in velocity magnitude across both sampling periods and in September, but not October (Table 4). The Mann-Whitney U test resulted in statistically significant differences in fish-selected versus available hydraulic conditions (depth and velocity values) for five of six tests (Table 5 and Fig. 7). This comparison suggests that fish prefer deeper sites, though this is likely driven by presence of relatively high conveyance values at sites with high rates of detection. The October analysis with only 40 observations could not distinguish between the two, indicating a sample size problem. Overall, the tests with the full dataset found that physical microhabitat conditions selected by fish were different from the overall available conditions at the river confluence, indicating a scientifically meaningful preference

Table 3
Total areas and percent occurrence for binned values of modeled depth and velocity magnitude occurring throughout the study area during September and October DIDSON sampling periods.

	Sept		Oct	
Depth Bin	Area (km^2)	%	Area (km^2)	%
0–1 m	0.08	12.9	0.27	46.1
1–2 m	0.30	45.7	0.25	42.7
2–3 m	0.22	33.4	0.06	9.6
3–4 m	0.04	6.8	0.01	1.0
4–5 m	0.01	0.8	< 0.01	0.6
> 5 m	< 0.01	0.4	0.00	0.0
Velocity magnitude bin	Area (km^2)	%	Area (km^2)	%
0–0.2 m/s	0.12	19.2	0.15	25.7
0.2–0.4 m/s	0.04	6.3	0.14	23.7
0.4–0.6 m/s	0.08	13.0	0.20	35.4
0.6–0.8 m/s	0.22	34.0	0.05	9.3
0.8–1.0 m/s	0.16	24.7	0.02	4.1
1.0–1.2 m/s	0.02	2.8	0.01	1.5
> 1.2 m/s	< 0.01	0.1	< 0.01	0.4

which is of interest to the topic of migration in river corridors.

3.1. Drivers of microhabitat selection

We reject H_{1b} as depth was not a statistically significant predictor of detection rate. However, F tests for all other predictor variables ($H_{1\text{-}a}$ and $H_{1c\text{-}g}$) and the multiple combinations yielded p values < 0.05 at 95% confidence (Table 6). Table 7 includes parameter estimates for these models. The best performing model (lowest AICc score) for predicting detection rate included a combination of conveyance, temperature, and turbidity, having a p value < 0.001, an adjusted r^2 value of 0.42, and a w value of 0.53 (an AVP is shown in Figure A.11 in the appendix). Fig. 8 includes graphical simulations of how this model behaves in predicting detection rate as a function of conveyance under three different temperature values while holding turbidity constant (steeper increases in D with increasing temperature, see panel a) and under three turbidity values while holding temperature constant (steeper increases in D with increasing turbidity, see panel b).

3.2. Drivers of migratory swimming behavior

We reject hypotheses $H_{2a\text{-}g}$. None of the candidate models yielded one or more statistically significant predictors of percent directed swimming behavior under the F test. However, turbidity ($H_{3\,f}$) as well as four combinations of predictors ($H_{3\,f}$) yielded statistically significant models for predicting percent milling behavior (see Table 8 for model performance metrics and Table 9 for parameter estimates). The best performing model for predicting percent milling behavior included all four hydraulic variables and had a p value < 0.001, an adjusted r^2 value of 0.82, and a w value of 0.83 (an AVP is shown in Figure A.12 in the

Table 4
A comparison of means and standard deviations for mean depth and velocity magnitude values associated with each DIDSON detection as well as sampled values from 2D hydrodynamic model outputs. Unsigned % differences between means and standard deviations of observed and modeled values are also included.

DIDSON sampling period	Summary statistic	Mean V_{mag} (m/s)	V_{mag} sample	|% V_{mag} diff.|	Mean d (m)	d sample (m)	|% d diff.|
All (N = 228)	Mean	0.48	0.50	3.26	2.25	1.57	30.3
	SD	0.26	0.28	9.29	0.50	0.84	66.0
Sept (N = 188)	Mean	0.52	0.57	8.85	2.35	1.83	22.1
	SD	0.25	0.30	18.40	0.44	0.89	104.1
Oct (N = 40)	Mean	0.29	0.43	48.99	1.80	1.11	38.4
	SD	0.16	0.23	43.76	0.56	0.53	5.7

Table 5
Results from Mann-Whitney U tests comparing mean depth and velocity magnitudes associated with each DIDSON detection with values randomly sampled from 2D hydrodynamic model outputs representing conditions in the study area outside of the DIDSON sample areas. The number of observed and modeled values were equal (Comparison N), and the comparison was performed for both September and October sampling periods combined as well as each period individually. Model cell N is the number of available depth or velocity values from which random samples were taken.

	Comparison N	Model cell N	Variable	U	p value
All	228	407979	V_{mag}	23,022	0.03
			depth	41,731	< 0.01
Sept	188	215515	V_{mag}	12,801	< 0.01
			depth	25,542	< 0.01
Oct	40	192463	V_{mag}	686	0.46
			depth	1151	< 0.01

appendix).

Velocity magnitude, Froude number, temperature, and four combinations of predictors yielded statistically significant models for predicting percent backtracking behavior (Tables 8 and 9). Temperature as a single predictor was found to be the best performing model and had a p value < 0.01, adjusted r^2 of 0.49, and w of 0.38. However, the combination of conveyance and temperature had a relatively low ΔAICc of 3.66, a p value of 0.02, and an r^2 value at 0.48. The two highest ranked models in this list (temperature and temperature/turbidity) dominated the weight of evidence, so the model with conveyance and temperature only received a w value of 0.06 (an AVP is shown in Figure A.13 in the appendix). We are highlighting this model because of our interest in hydraulic variables as drivers of migratory habitat selection and behavior. Fig. 9 includes a graphical simulation demonstrating an inverse relationship between percent backtracking behavior and conveyance which is consistent with our finding that greater conveyance values are favored in micro-scale movements.

4. Discussion

4.1. Habitat selection

The large difference in adult Chinook salmon detections between September and October sampling periods corresponds with the considerable difference in combined discharge and associated hydraulic changes at the confluence between September and October (237 m^3/s and 85 m^3/s, respectively). This result is consistent with the general understanding of the important role that mainstem river discharge magnitude and timing play in the upstream migration of Chinook

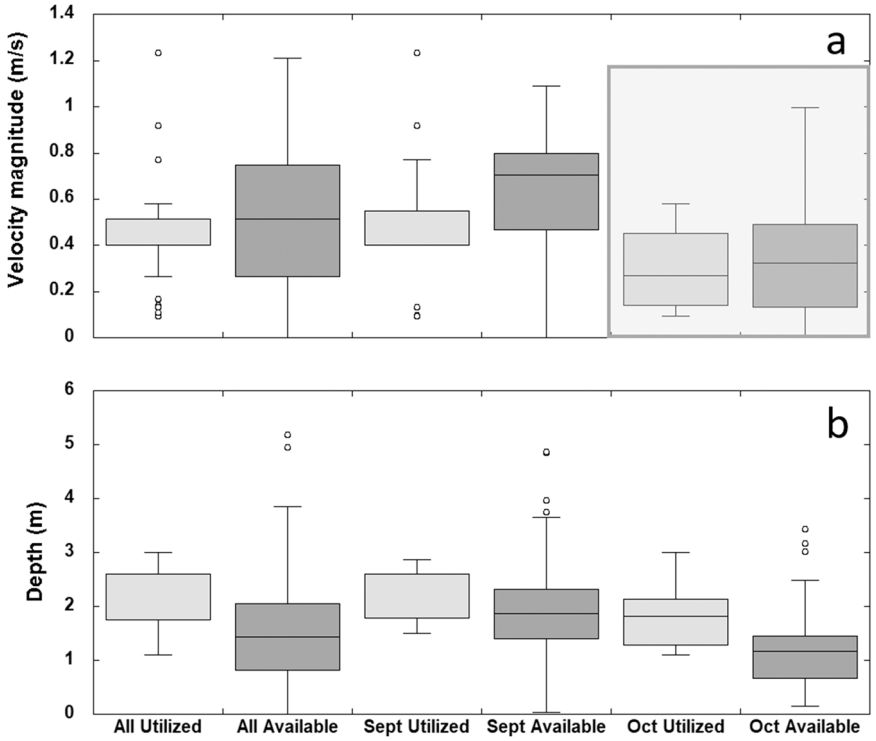

Fig. 7. Box and whisker plot showing a comparison of velocity magnitude (panel a) and depth (panel b) values utilized in DIDSON detections and randomly sampled modeled values from 2D hydrodynamic outputs representing available conditions outside of DIDSON sample sites. The gray box indicates the Mann-Whitney U test comparison that was not statistically significant at 95% confidence.

Table 6
Model performance summary and AICc ranking for nonlinear regression models predicting detection rate.

Rank	Model	K	d.f.	F stat	p value	AICc	ΔAICc	Adjusted r^2	w
1	D ~ C + T + TU	5	25	7.90	**< 0.001**	104.58	0.00	0.42	0.53
2	D ~ C	3	27	13.24	**< 0.01**	106.68	2.11	0.30	0.19
3	D ~ T + TU	4	26	7.54	**< 0.01**	107.70	3.12	0.32	0.11
4	D ~ C + T	4	26	7.14	**< 0.01**	108.28	3.70	0.30	0.08
5	D ~ V_{mag}	3	27	9.24	**< 0.01**	109.72	5.14	0.23	0.04
6	D ~ Fr	3	27	7.00	**0.01**	111.57	7.00	0.18	0.02
7	D ~ T	3	27	6.42	**0.02**	112.07	7.50	0.16	0.01
8	D ~ TU	3	27	4.62	**0.04**	113.68	9.11	0.11	0.01
9	D ~ V_{mag} + d + C +Fr + T + TU	8	22	3.74	**0.01**	114.09	9.51	0.37	< 0.01
10	D ~ V_{mag} + d + C + Fr	6	24	3.34	**0.02**	114.14	9.56	0.25	< 0.01
11	D ~ d	3	27	0.25	0.62	117.99	13.41	< 0.00	< 0.01

K = number of parameters, d.f. = degrees of freedom, AICc = Akaike information criterion corrected for small sample sizes, ΔAICc = increase in AICc score from the top-ranked model, Adjusted r^2 is the coefficient of determination adjusted for all predictors, w is the relative weight of support for each model among the candidate set. D = detection rate, Vmag = velocity magnitude, d = depth, C = conveyance, Fr = Froude number, T = temperature, TU = turbidity. P values in bold indicate statistical significance at 95% confidence.

Table 7
Model parameter estimates for statistically significant candidate models predicting detection rate.

AICc Rank	Model	Intercept (α)	β_{Vmag}	β_d	β_C	β_{FR}	β_T	β_{TU}
1	$D = e^{(\beta_C C+\beta_T T+\beta_{TU} TU+\alpha)}$	-12.87			1.27		0.41	0.51
2	$D = e^{(\beta_C C+\alpha)}$	-5.41			1.77			
3	$D = e^{(\beta_T T+\beta_{TU} TU+\alpha)}$	-17.55					0.78	0.58
4	$D = e^{(\beta_C C+\beta_T T+\alpha)}$	-9.75			1.46		0.31	
5	$D = e^{(\beta_{Vmag} V_{mag}+\alpha)}$	-5.14	2.57					
6	$D = e^{(\beta_{Fr} Fr+\alpha)}$	-4.96				8.85		
7	$D = e^{(\beta_T T+\alpha)}$	-14.75					0.73	
8	$D = e^{(\beta_{TU} TU+\alpha)}$	-5.85						0.53
9	$D = e^{(\beta_{Vmag} V_{mag}+\beta_d d+\beta_C C+\beta_{Fr} Fr+\beta_T T+\beta_{TU} TU+\alpha)}$	-13.27	26.76	0.00081	-3.55	-75.67	0.44	0.56
10	$D = e^{(\beta_{Vmag} V_{mag}+\beta_d d+\beta_C C+\beta_{Fr} Fr+\alpha)}$	-3.59	-4.35	-0.89	4.13	-0.13		

D = detection rate, Vmag = velocity magnitude, d = depth, C = conveyance, Fr = Froude number, T = temperature, TU = turbidity.

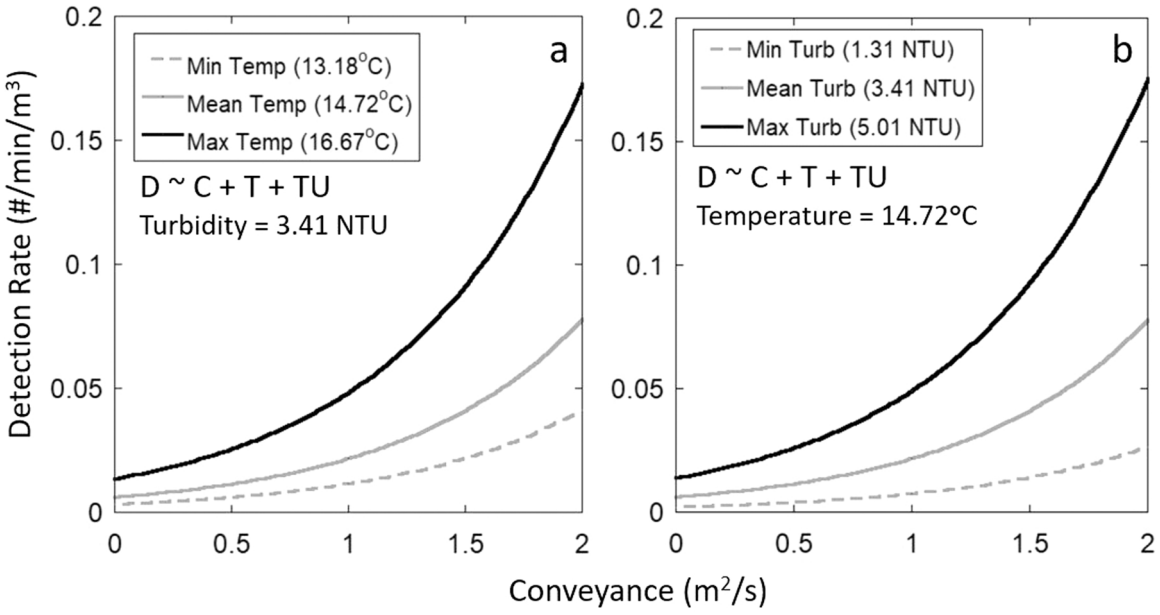

Fig. 8. Detection rate is predicted using the highest AICc-ranked model which is fit using a nonlinear (exponential) regression and includes conveyance, temperature, and turbidity as predictors. Each panel includes continuous predictions of detection rate as a function of conveyance. Panel a includes three different temperature values that correspond to the maximum, minimum, and mean values in our observed data. Turbidity is held constant at the mean observed value in our data. Panel b uses this same scheme but with three turbidity values used and temperature held at the observed mean.

salmon, particularly in the California Central Valley (Hasler et al., 2014). However, this study investigated the role of microhabitat variables driven by discharge and acting as migratory navigation cues. Simply pointing to discharge magnitude as a navigation cue does not mechanistically characterize migratory behavioral responses. The comparison of depth and velocity magnitude conditions selected vs. those available throughout the study area at the time of observation showed statistically significant differences in mean values, indicating

Table 8
Model performance summary and AICc ranking for regression models predicting frequency of (1) directed, (2) milling, and (3) backtracking swimming behaviors.

Directed									
Rank	Model	K	d.f.	F stat	p value	AICc	ΔAICc	Adjusted r^2	w
1	$P_d \sim d$	3	21	2.42	0.15	224.13	0.00	0.05	0.27
2	$P_d \sim T$	3	21	1.89	0.18	224.49	0.35	0.04	0.23
3	$P_d \sim Fr$	3	21	0.41	0.53	226.02	1.89	< 0.00	0.10
4	$P_d \sim C$	3	21	0.20	0.66	226.25	2.12	< 0.00	0.09
5	$P_d \sim TU$	3	21	0.18	0.68	226.27	2.14	< 0.00	0.09
6	$P_d \sim V_{mag}$	3	21	0.06	0.81	226.40	2.27	< 0.00	0.09
7	$P_d \sim T + TU$	4	20	0.98	0.39	227.27	3.14	< 0.00	0.06
8	$P_d \sim C + T$	4	20	0.90	0.42	227.44	3.31	< 0.00	0.05
9	$P_d \sim C + T + TU$	5	19	0.63	0.61	230.56	6.42	< 0.00	0.01
10	$P_d \sim V_{mag} + d + C + Fr$	6	18	1.23	0.33	230.89	6.75	0.04	0.01
11	$P_d \sim V_{mag} + d + C + Fr + T + TU$	8	16	1.07	0.42	237.75	13.62	0.02	< 0.01
Milling									
Rank	Model	K	d.f.	F stat	p value	AICc	ΔAICc	Adjusted r^2	w
1	$P_m \sim V_{mag} + d + C + Fr$	6	9	15.47	**< 0.001**	135.79	0.00	0.82	0.83
2	$P_m \sim TU$	3	12	11.9	**< 0.01**	139.44	3.64	0.46	0.13
3	$P_m \sim T + TU$	4	11	5.86	**0.02**	142.98	7.18	0.43	0.02
4	$P_m \sim d$	3	12	3.35	0.09	145.64	9.84	0.15	0.01
5	$P_m \sim Fr$	3	12	2.85	0.12	146.10	10.31	0.12	< 0.01
6	$P_m \sim V_{mag}$	3	12	1.65	0.22	147.28	11.49	0.05	< 0.01
7	$P_m \sim C + T + TU$	5	10	3.68	**0.05**	147.76	11.97	0.38	< 0.01
8	$P_m \sim C$	3	12	0.10	0.76	148.97	13.18	< 0.00	< 0.01
9	$P_m \sim T$	3	12	0.01	0.91	149.07	13.27	< 0.00	< 0.01
10	$P_m \sim V_{mag} + d + C + Fr + T + TU$	8	7	12.61	**< 0.01**	150.92	15.13	0.84	< 0.01
11	$P_m \sim C + T$	4	11	0.31	0.74	152.36	16.57	-0.12	< 0.01
Backtracking									
Rank	Model	K	d.f.	F stat	p value	AICc	ΔAICc	Adjusted r^2	w
1	$P_b \sim T$	3	10	11.64	**< 0.01**	112.12	0.00	0.49	0.38
2	$P_b \sim T + TU$	4	9	9.78	**< 0.01**	112.23	0.12	0.62	0.36
3	$P_b \sim C + T$	4	9	6.13	**0.02**	115.78	3.66	0.48	0.06
4	$P_b \sim Fr$	3	10	5.82	**0.04**	115.87	3.76	0.30	0.06
5	$P_b \sim V_{mag}$	3	10	5.52	**0.04**	116.10	3.99	0.29	0.05
6	$P_b \sim Con$	3	10	4.50	0.06	116.92	4.81	0.24	0.03
7	$P_b \sim TU$	3	10	4.10	0.07	117.26	5.14	0.22	0.03
8	$P_b \sim C + T + TU$	5	8	6.00	**0.02**	118.23	6.12	0.58	0.02
9	$P_b \sim d$	3	10	1.40	0.27	119.81	7.70	0.03	0.01
10	$P_b \sim V_{mag} + d + C + Fr$	6	7	4.78	**0.04**	125.37	13.25	0.58	< 0.01
11	$P_b \sim V_{mag} + d + C + Fr + T + TU$	8	5	3.98	0.08	155.32	43.21	0.62	< 0.01

K = number of parameters, d.f. = degrees of freedom, AICc = Akaike information criterion corrected for small sample sizes, ΔAICc = increase in AICc score from the top-ranked model, Adjusted r^2 is the coefficient of determination adjusted for all predictors, w is the relative weight of support for each model among the candidate set. Px = percent of behavior among detections (d = directed, m = milling, b = backtracking), Vmag = velocity magnitude, d = depth, C = conveyance, Fr = Froude number, T = temperature, TU = turbidity. P values in bold indicate statistical significance at 95% confidence.

Table 9
Model parameter estimates for statistically significant candidate models predicting percent milling and backtracking behaviors.

AICc Rank	Model	Intercept (α)	β_{Vmag}	β_d	β_C	β_{FR}	β_T	β_{TU}
1	$P_m = \beta_{Vmag}V_{mag} + \beta_d d + \beta_C C + \beta_{Fr}Fr + \alpha$	-234.44	1732.46	180.20	-693.47	-2467.93		
2	$P_m = \beta_{TU}TU + \alpha$	140.62						-23.23
3	$P_m = \beta_T T + \beta_{TU}TU + \alpha$	243.26					-6.76	-23.84
7	$P_m = \beta_C C + \beta_T T + \beta_{TU}TU + \alpha$	137.67			-14.19		1.60	-25.40
10	$P_m = \beta_{Vmag}V_{mag} + \beta_d d + \beta_C C + \beta_{Fr}Fr + \beta_T T + \beta_{TU}TU + \alpha$	80.58	630.14	129.76	-389.16	-44.56	-2.55	-11.90
1	$P_b = \beta_T T + \alpha$	346.60					-20.87	
2	$P_b = \beta_T T + \beta_{TU}TU + \alpha$	345.21					-18.35	-9.68
3	$P_b = \beta_C C + \beta_T T + \alpha$	305.03			-12.43		-17.35	
4	$P_b = \beta_{Fr}Fr + \alpha$	64.46				-233.58		
5	$P_b = \beta_{Vmag}V_{mag} + \alpha$	65.62	-56.42					
8	$P_b = \beta_C C + \beta_T T + \beta_{TU}TU + \alpha$	369.77			7.43		-19.92	-11.70
10	$P_b = \beta_{Vmag}V_{mag} + \beta_d d + \beta_C C + \beta_{Fr}Fr + \alpha$	16.07	4322.14	28.83	-744.25	-12729.9		

Px = percent of behavior among detections (m = milling, b = backtracking), Vmag = velocity magnitude, d = depth, C = conveyance, Fr = Froude number, T = temperature, TU = turbidity.

that non-random microhabitat selection did occur.

It is particularly interesting that even though fish were attracted to higher discharge, they were attracted to lower velocity. One interpretation is that the fish may have been observed in holding locations, essentially pausing on their journey for any one of several reasons, including some awareness of the confluence itself. Another interpretation is that the direct hydraulic variable driving migratory behavior is conveyance, as our regression analysis suggests. This variable includes both depth and velocity components, meaning that neither can be analyzed independently of the other in this context. For example, our results suggest that greater swim depths are preferred, as long as there is adequate velocity present as well for rheotactic orientation.

Results indicate that localized conveyance is likely the missing intermediate variable translating channel-wide discharge into local

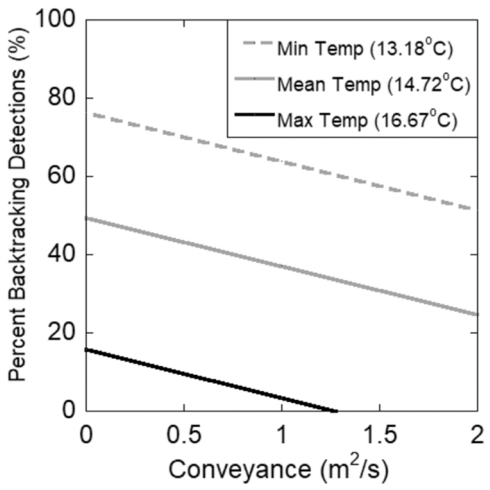

Fig. 9. Percent backtracking behavior is predicted using the third highest AICc-ranked model which is fit using a linear regression and includes conveyance and temperature as predictors. The plot includes continuous predictions of percent backtracking as a function of conveyance using the maximum, minimum, and mean values for temperature from our observed data.

hydraulics that fish experience and thus is an important driver of habitat selection, which can help explain some of the patterns of detection seen in Table 2. Overall, the Feather zone experienced the most detections. From a hydraulics perspective, this can be attributed to the greatest combined values of depth and velocity to yield high conveyance throughout that zone. Furthermore, the deep sites experienced the most overall detections and even though they did not all experience high velocities (Fig. 4), localized cross-sectional area resulted in higher conveyance values. Conveyance was included in our best performing regression model for predicting detection rate and was ranked second-best as a singular predictive variable. This is compelling evidence that conveyance plays an important role in instantaneous micro-scale habitat selection during adult upstream migration in Chinook salmon. However, it does not completely dictate microhabitat selection among individuals.

Temperature and turbidity were also included as predictors and as mentioned in our study design, these micro-scale attributes cannot be disentangled from acting as indicators of natal source water and homing fidelity in our observations. Therefore, it is likely that homing occurs in conjunction with responses to hydraulic flow features. In some cases, hydraulics may significantly influence navigational cues in migration as has been seen previously in this particular system (YARMT, 2013).

Upstream migration by adult salmon involves constant compromise between bioenergetic cost of movement and fidelity to navigational cues, one of which is rheotaxis. Olfactory cues aside, an individual may choose the least energetically costly path through a channel network (deep, slow-moving areas), but they may lack a velocity field with sufficient magnitude and direction necessary to facilitate sufficient rheotactic orientation (Coombs et al., 2020). Likewise, choosing to occupy shallow, fast-moving areas is energetically costly and may result in exposure to turbulent flow structures of the same size as an individual fish shed by flow interacting with local features, such as large substrate particles, deposited wood, bedforms, and man-made structures (Harvey and Clifford, 2009). The avoidance of turbulent eddies of the same size as an individual fish has been documented in fishway studies (Silva et al., 2012) and such eddies may be more common in fast, shallow areas. Avoidance of turbulence may be due to energetic constraint rather than interference with rheotaxis, as turbulence has been shown to negatively affect fish swim speed and increase energetic cost (Enders et al., 2003; Lupandin, 2005).

The results of the hand-held temperature and turbidity surveys (Fig. 5) illustrate the overall thermal and optical condition of the two rivers during each DIDSON deployment period. In both periods, the LYR tended to be clearer than the LFR and the difference persisted throughout the study area with minimal mixing occurring before the downstream boundary (lateral differences at the downstream-most sampling stations in September and October of approximately 1.5 NTU and 1 NTU, respectively). It is unlikely that the range of turbidity values observed throughout this study were great enough to affect migratory behavior alone (Bjornn and Reiser, 1991). Although we found it to be a significant predictor of habitat selection, there are likely other covariates at play that act as more important micro-scale navigational cues. Surface temperature differences between the two rivers changed dramatically between the two sampling periods. In September, the LFR was cooler and a dramatic lateral difference in temperature at the confluence junction can be seen before the LFR begins to thermally influence the east side of the channel toward the downstream boundary. This difference in temperature may have played a role in the differences in reach-scale habitat selection during this period (Table 2), deterring Feather-origin fish from entering the LYR (consistent with the findings of thermal influence on migratory routing in this system by the YARMT). In the October period, the thermal condition switched; the LYR was cooler than the LFR and minimal mixing appeared to occur within the study area. The increase of temperature in the LFR is likely a result of the decrease in discharge combined with warm water input upstream of the study area at the Thermalito Afterbay outlet. Rates of detection changed very little among the three zones in the October period (Table 2), indicating that a thermal barrier at the confluence may potentially deter Feather-origin fish from entering the LYR.

4.2. Swimming behavior

Comparisons of swimming behavior type by sampling period, zone, and site type all show most detections to be exhibiting directed movement with 135 detections overall (Table 2). Milling and backtracking behavior occurred to a much lesser extent with 39 and 54 detections, respectively. It should be noted that these behaviors were not tracked through space beyond the DIDSON's field of view, so they cannot be used to characterize longitudinal movements within the study area. However, they do provide some indication of relative movement among detections. Because most individuals selected the LFR, we expected the majority of directed movement to occur in that zone. Our regression analysis did not provide an adequate model for predicting directed movement, suggesting that although salmon appear to have preferences for migratory microhabitats, upstream movement may occur in a wide variety of hydraulic, thermal, and optical conditions.

However, we did identify predictors for milling and backtracking behavior. This is more useful from a management perspective because it can be assumed that the majority of fish will be progressing upstream, but it may be possible to strategically minimize conditions that deter upstream movement via top-down controls on localized hydraulics such as discharge magnitude and ratio at a confluence. Our analysis suggests that milling occurs in response to localized hydraulics whereas backtracking may occur partially in response to hydraulics but is also influenced by temperature and turbidity where the presence or absence of olfactory homing cues may be at play. Although both our microhabitat selection and behavioral results show conveyance as the best hydraulic predictor variable for migratory habitat selection and movement, Moir et al. (2002) suggests that Froude number may be a better indicator for assessing salmonid habitat suitability for multiple body lengths due to its flexibility and scale-independent nature as a dimensionless value. In the absence of a clear biological mechanism for behavioral response to either cue, it may be useful to analyze both variables, depending on the applied research or management context.

4.3. Study limitations and implications of outlier data

While our DIDSON sampling scheme was designed to account for as many environmental drivers of habitat selection as possible, we could

not account for all of them (Fig. 1). The importance of olfactory navigation cues is well understood in the literature and likely played a role in the greater rates of detection in the LFR relative to the LYR across both sampling periods. The addition of a water chemistry analysis at the confluence could have allowed us to attribute patterns in micro-scale habitat selection to olfactory homing via micro-scale concentrations of key odor compounds distributed through space and time. Also, due to logistical constraints, we were not able to sample at night and thus could not quantify the effect of photoperiod on migratory movements. Finally, there was also some uncertainty in species identification as the DIDSON sampling approach only provided acoustic data with limited details of fish body morphology. Body length served as our primary criteria for species identification (see Section 2.6 of the appendix for details). An alternative approach would have been to measure tail beat frequencies of individual fish returns using an approach such as the one developed by Mueller et al. (2010) for differentiating salmon species. However, we did not have access to the computing resources necessary to undertake this analysis.

Our DIDSON surveys resulted in a very wide range of detection rates among the sample sites that included ≥ 1 salmon detection (0.001–1.87 #/min/m^3). As discussed in Section 2.5 of the appendix, we did not find any sampling bias based on the volume sampled per deployment, the duration of each deployment, the time of day that each deployment occurred, or the mean body length estimate observed in each deployment. However, one deployment (deployment 2 at site FD2 in September) did experience an exceptionally high rate of detection (1.87 #/min/m^3) and accounted for 48% of detections in our study. This is an order of magnitude greater than the next highest detection rate value (0.27 #/min/m^3 at FS2 in September).

Salmon were detected in 34 out of 48 total deployments, though five of those were omitted because we could not collect corresponding velocity data. Of the 29 usable sites where detections occurred, only eight experienced detection rates > 0.05 #/min/m^3, accounting for 69% of all detections. All eight of these occurred during the September period in either the Feather zone or the downstream zone. Mean conveyance values among these eight deployments ranged from 0.86 m^2/s to 1.85 m^2/s. Deployment 2 at the FD2 site had a mean conveyance value of 1.05 m^2/s, falling in the lower end of this range. However, it is notable that this deployment had the lowest temperature and highest turbidity values (15.15 °C and 5.01 NTU) among these eight deployments which ranged from 15.15° to 16.0°C and 1.57 – 5.01 NTU.

Since the detections in the second September FD2 deployment represented 48% of our data, the corresponding habitat attributes had a disproportionate influence on our detection rate models. The temperature and turbidity values observed at FD2 likely resulted in the inclusion of these variables in our best performing regression model and biases our findings regarding thermal and optical habitat preferences. However, the fact that the mean conveyance value for the second FD2 deployment was within the range of the other sites with relatively high detection rates is very encouraging. This suggests that the conditions at FD2 are representative of true hydraulic microhabitat preferences, and data from that site did not introduce a misleading bias in our results with respect to the hydraulic component of our study. It is difficult to identify a single reason for the anomalous detection rate for the second September FD2 deployment. It is likely that there was density-dependent movement occurring at that time and location, and we happened to capture it at a location that was representative of the favorable hydraulic conditions in the study area.

4.4. Scientific and management implications

We see patterns in preference for specific fine-scale hydraulic conditions along the migratory pathway and indications that hydraulics are a partial driver of migratory swimming behavior. Discharge magnitude has traditionally been used as a proxy for the timing of migration initiation and upstream movement (Hasler et al., 2014; Quinn, 2018; Rand et al., 2006) and recent work shows that there may also be complex social interactions that drive upstream movement as well (Berdahl et al., 2017, 2016). However, fine details of upstream movement cannot be inferred from these large-scale phenomena. In many regions, flows are regulated, and flow schedules are carefully crafted annually to accommodate competing social, economic, and environmental demands. How flows translate into local hydraulics cannot be inferred but requires an assessment of the sub-reach-scale topographic regime, especially at the complex, vital locations that river confluences present to migratory fish. Understanding fine-scale patterns of migratory movement of adult salmon at confluences may be essential to their long-term conservation and survival by providing tools to minimize high rates of straying in imperiled populations occurring in managed river networks.

One reason to be optimistic about the future of river management for salmon is that we have witnessed major technological advancements in recent decades that allow for wholesale characterization and assessment of riverine habitats. LiDAR and multibeam sonar are examples of survey technology that allow for gathering highly detailed topographies as well as information on sediment composition and vegetation cover. Computational fluid dynamics modeling has advanced significantly with access to ever-growing computing power, allowing for detailed and accurate simulations of open-channel hydraulics in a variety of aquatic settings. The field of ecohydraulics has already adopted these technologies to assess habitat availability and function for specific lifecycle stages of anadromous salmonids (Kammel et al., 2016; Moniz et al., 2019; Wheaton et al., 2018). There is little existing literature on coupling hydraulic and thermal attributes at a microhabitat scale and more work is needed before these mechanisms can be modeled concurrently (Ouellet et al., 2020).

CRediT authorship contribution statement

Sean Luis: Conceptualization, Methodology, Formal analysis, Investigation, Writing – original draft, Visualization, Project administration, Funding acquisition. **Gregory Pasternack:** Conceptualization, Resources, Data curation, Writing – review & editing, Supervision.

Declaration of Competing Interest

The authors declare that they have no known competing financial interests or personal relationships that could have appeared to influence the work reported in this paper.

Data availability

Data will be made available on request.

Acknowledgements

This project was financially supported by the Bob Wisecarver Memorial Scholarship awarded by the Diablo Valley Fly Fishermen; Small Projects Grant awarded by the Western Division of the American Fisheries Society; and Henry A. Jastro Graduate Research Award awarded by the University of California Davis. Student funding was also provided through the Chapter 33 Post 9/11 G.I. Bill through the U.S. Department of Veterans Affairs. This project was also supported by the USDA National Institute of Food and Agriculture, Hatch project number CA-D-LAW-7034-H. The authors would like to thank the Pacific States Marine Fisheries Commission; California Department of Fish and Wildlife; California Department of Water Resources; and the City of Marysville for logistical support, equipment and personnel loans, and data collaboration. Finally, we would like to dedicate this paper to Dr. Ethan Mora who provided key advice during planning stages and unfortunately passed away during this project.

Appendix A. Supporting information

Supplementary data associated with this article can be found in the online version at doi:10.1016/j.fishres.2023.106634.

References

Acreman, M., Aldrick, J., Binnie, C., Black, A., Cowx, I., Dawson, H., Dunbar, M., Extence, C., Hannaford, J., Harby, A., Holmes, N., Jarritt, N., Old, G., Peirson, G., Webb, J., Wood, P., 2009. Environmental flows from dams: the water framework directive. Proc. Inst. Civ. Eng. Eng. Sustain. 162, 13–22. https://doi.org/10.1680/ensu.2009.162.1.13.

Ahmad, S.K., Hossain, F., 2020. Realizing ecosystem-safe hydropower from dams. Renewables 7, 2. https://doi.org/10.1186/s40807-020-00060-9.

Anderson, D.R., Burnham, K.P., 2002. Avoiding pitfalls when using information-theoretic methods. J. Wildl. Manag. 66, 912–918. https://doi.org/10.2307/3803155.

Anderson, J.J., Beer, W.N., 2009. Oceanic, riverine, and genetic influences on spring chinook salmon migration timing. Ecol. Appl. 19, 1989–2003. https://doi.org/10.1890/08-0477.1.

Yuba Accord River Management Team, 2013. Aquatic Resources of the Lower Yuba River: Past, Present, and Future (Draft Interim Report). Yuba Accord Monitoring and Evaluation Program.

National Marine Fisheries Service, 2016. Endangered Species Act Section 7(a)(2) Biological Opinion, and Magnuson-Stevens Fishery Conservation and Management Act Essential Fish Habitat Response and Fish and Wildlife Coordination Act Recommendations for Relicensing the Oroville Facilities Hydroelectric Project, Butte County California FERC Project No. 2100–134).

California Department of Fish and Wildlife, 2022. Fisheries Branch Anadromous Assessment – GrandTab. Annual Report.

Ayllón, D., Almodóvar, A., Nicola, G.G., Elvira, B., 2009. Interactive effects of cover and hydraulics on brown trout habitat selection patterns. River Res. Appl. 25, 1051–1065. https://doi.org/10.1002/rra.1215.

Baldes, R.J., Vincent, R.E., 1969. Physical parameters of microhabitats occupied by brown trout in an experimental flume. Trans. Am. Fish. Soc. 98, 230–238. https://doi.org/10.1577/1548-8659(1969)98[230:PPOMOB]2.0.CO;2.

Baumgartner, L.J., Reynoldson, N., Cameron, L., Stanger, J., 2006. Assessment of a Dual-frequency Identification Sonar (DIDSON) for application in fish migration studies (No. 84), NSW Department of Primary Industries - Fisheries Final Report Series. NSW Department of Primary Industries, New South Wales, Australia.

Belcher, E., Matsuyama, B., Trimble, G., 2001. Object identification with acoustic lenses, in: MTS/IEEE Oceans 2001. An Ocean Odyssey. Conference Proceedings (IEEE Cat. No.01CH37295). Presented at the Oceans 2001. An Ocean Odyssey., Marine Technol. Soc., Honolulu, HI, USA, pp. 6–11. ⟨https://doi.org/10.1109/OCEANS.2001.968656⟩.

Belcher, E., Hanot, W., Burch, J., 2002. Dual-Frequency Identification Sonar (DIDSON), in: Proceedings of the 2002 Interntional Symposium on Underwater Technology (Cat. No.02EX556). Presented at the 2002 International Symposium on Underwater Technology, IEEE, Tokyo, Japan, pp. 187–192. ⟨https://doi.org/10.1109/UT.2002.1002424⟩.

Benda, L., Andras, K., Miller, D., Bigelow, P., 2004. Confluence effects in rivers: Interactions of basin scale, network geometry, and disturbance regimes: effects of confluences on river morphology. Water Resour. Res 40. https://doi.org/10.1029/2003WR002583.

Berdahl, A., Westley, P.A.H., Levin, S.A., Couzin, I.D., Quinn, T.P., 2016. A collective navigation hypothesis for homeward migration in anadromous salmonids. Fish Fish 17, 525–542. https://doi.org/10.1111/faf.12084.

Berdahl, A., Westley, P.A.H., Quinn, T.P., 2017. Social interactions shape the timing of spawning migrations in an anadromous fish. Anim. Behav. 126, 221–229. https://doi.org/10.1016/j.anbehav.2017.01.020.

Best, J.L., 1986. The morphology of river channel confluences. Prog. Phys. Geogr.: Earth Environ. 10, 157–174. ⟨https://doi.org/10.1177/030913338601000201⟩.

Bjornn, T.C., Reiser, D.W., 1991. Habitat Requirements of Salmonids in Streams, in: Influences of Forest and Rangeland Management on Salmonid Fishes and Their Habitat. Am. Fish. Soc. Special Publication, pp. 83–138.

Blettler, M.C.M., Amsler, M.L., Ezcurra de Drago, I., Drago, E., Paira, A., Espinola, L.A., Eberle, E., Szupiany, R., 2016. Fine sediment input and benthic fauna interactions at the confluence of two large rivers. Int. J. Environ. Res 10. https://doi.org/10.22059/ijer.2016.56889.

Bradford, M.J., Higgins, P.S., Korman, J., Sneep, J., 2011. Test of an environmental flow release in a British Columbia river: does more water mean more fish?: Test of environmental flow release. Freshw. Biol. 56, 2119–2134. https://doi.org/10.1111/j.1365-2427.2011.02633.x.

Brown, L.R., Ford, T., 2002. Effects of flow on the fish communities of a regulated California river: implications for managing native fishes. River Res. Appl. 18, 331–342. https://doi.org/10.1002/rra.673.

Brown, R.A., Pasternack, G.B., 2009. Comparison of methods for analysing salmon habitat rehabilitation designs for regulated rivers. River Res. Appl. 25, 745–772. https://doi.org/10.1002/rra.1189.

Buddendorf, W.B., Malcolm, I.A., Geris, J., Wilkinson, M.E., Soulsby, C., 2017. Metrics to assess how longitudinal channel network connectivity and in-stream Atlantic salmon habitats are impacted by hydropower regulation. Hydrol. Process. 31, 2132–2142. https://doi.org/10.1002/hyp.11159.

California Department of Water Resources, California Department of Fish and Game, 1983. Agreement Concerning the Operation of the Oroville Division of the State Water Project. for Management of Fish and Wildlife.

Carnie, R., Tonina, D., McKean, J.A., Isaak, D., 2016. Habitat connectivity as a metric for aquatic microhabitat quality: application to Chinook salmon spawning habitat: Habitat Connectivity. Ecohydrol 9, 982–994. https://doi.org/10.1002/eco.1696.

Cavanaugh, J.E., Neath, A.A., 2019. The Akaike information criterion: Background, derivation, properties, application, interpretation, and refinements. WIREs Comp. Stat. 11. https://doi.org/10.1002/wics.1460.

Church, M., 2006. Bed material transport and the morphology of alluvial river channels. Annu. Rev. Earth Planet. Sci. 34, 325–354. https://doi.org/10.1146/annurev.earth.33.092203.122721.

Coombs, S., Bak-Coleman, J., Montgomery, J., 2020. Rheotaxis revisited: a multi-behavioral and multisensory perspective on how fish orient to flow. J. Exp. Biol. 223, jeb223008. https://doi.org/10.1242/jeb.223008.

Dahl, J., Dannewitz, J., Karlsson, L., Petersson, E., Löf, A., Ragnarsson, B., 2004. The timing of spawning migration: implications of environmental variation, life history, and sex. Can. J. Zool. 82, 1864–1870. https://doi.org/10.1139/z04-184.

Dietrich, W.E., Bellugi, D.G., Sklar, L.S., Stock, J.D., Heimsath, A.M., Roering, J.J., 2003. Geomorphic Transport Laws for Predicting Landscape form and Dynamics. In: Wilcock, P.R., Iverson, R.M. (Eds.), Geophysical Monograph Series. American Geophysical Union, Washington, D. C, pp. 103–132. ⟨https://doi.org/10.1029/135GM09⟩.

Dittman, A., Quinn, T., 1996. Homing in Pacific salmon: mechanisms and ecological basis. J. Exp. Biol. 199, 83–91.

Doyle, M.W., Ensign, S.H., 2009. Alternative reference frames in river system science. BioSci 59, 499–510. https://doi.org/10.1525/bio.2009.59.6.8.

Edwards, P.J., Williard, K.W.J., Schoonover, J.E., 2015. Fundamentals of watershed hydrology. J. Contemp. Water Res. Educ. 154, 3–20. https://doi.org/10.1111/j.1936-704X.2015.03185.x.

Enders, E.C., Boisclair, D., Roy, A.G., 2003. The effect of turbulence on the cost of swimming for juvenile Atlantic salmon (Salmo salar). Can. J. Fish. Aquat. Sci. 60, 1149–1160. https://doi.org/10.1139/f03-101.

Fangue, N.A., Cocherell, D.E., Mauduit, F., Poletto, J.B., Carr, K., O'Rear, T.A., Soyster, G., Lorenzato, S., Carlon, J., Kavvas, M.L., Cech, J.J., 2021. Juvenile Chinook salmon use of sandbar willows in a large-scale, simulated riparian floodplain: microhabitat and energetics. Environ. Biol. Fish. 104, 867–879. https://doi.org/10.1007/s10641-021-01119-2.

Faulkner, A.V., Maxwell, S.L., 2009. An Aiming Protocol for Fish-Counting Sonars using River Bottom Profiles from a Dual-Frequency Identification Sonar (DIDSON) (Fishery Manuscript No. 09–03), Divisions of Sport Fish and Commercial Fisheries. Alaska Department of Fish and Game.

Favrot, S.D., Jonasson, B.C., Peterson, J.T., 2018. Fall and winter microhabitat use and suitability for spring chinook salmon Parr in a U.S. Pacific Northwest River. Trans. Am. Fish. Soc. 147, 151–170. https://doi.org/10.1002/tafs.10011.

Fox, J., Weisberg, S., Price, B., Adler, D., Bates, D., Baud-Bovy, G., Bolker, B., Ellison, S., Firth, D., Friendly, M., Gorjane, G., Graves, S., Heiberger, R., Krivitsky, P., Laboissiere, R., Maechler, M., Monette, G., Murdoch, D., Nilsson, H., Ogle, D., Ripley, B., Venables, W., Walker, S., Winsemius, D., Zeileis, A., R. Core Team, 2022. Companion to Applied Regression, R Package (Version 3.0–13). ⟨https://CRAN.R-project.org/package=car⟩.

Gendaszek, A.S., Burton, K., Magirl, C.S., Konrad, C.P., 2018. Streambed scour of salmon spawning habitat in a regulated river influenced by management of peak discharge. Freshw. Biol. 63, 917–927. https://doi.org/10.1111/fwb.12987.

Gervasi, A.A., Pasternack, G.B., East, A.E., 2021. Flooding duration and volume more important than peak discharge in explaining 18 years of gravel–cobble river change. Earth Surf. Process. Land. 46, 3194–3212. https://doi.org/10.1002/esp.5230.

Goniea, T.M., Keefer, M.L., Bjornn, T.C., Peery, C.A., Bennett, D.H., Stuehrenberg, L.C., 2006. Behavioral Thermoregulation and Slowed Migration by Adult Fall Chinook Salmon in Response to High Columbia River Water Temperatures. Transactions of the American Fisheries Society 135, 408–419. https://doi.org/10.1577/T04-113.1.

Gualtieri, C., Ianniruberto, M., Filizola, N., Santos, R., Endreny, T., 2017. Hydraulic complexity at a large river confluence in the Amazon basin. Ecohydrology 10, e1863. https://doi.org/10.1002/eco.1863.

Harvey, G.L., Clifford, N.J., 2009. Microscale hydrodynamics and coherent flow structures in rivers: Implications for the characterization of physical habitat. River Res. Appl. 25, 160–180. https://doi.org/10.1002/rra.1109.

Hasler, C.T., Guimond, E., Mossop, B., Hinch, S.G., Cooke, S.J., 2014. Effectiveness of pulse flows in a regulated river for inducing upstream movement of an imperiled stock of Chinook salmon. Aquat. Sci. 76, 231–241. https://doi.org/10.1007/s00027-013-0332-5.

High, B., Peery, C.A., Bennett, D.H., 2006. Temporary Staging of Columbia River Summer Steelhead in Coolwater Areas and Its Effect on Migration Rates. Transactions of the American Fisheries Society 135, 519–528. https://doi.org/10.1577/T04-224.1.

Holvoet, K.M.A., Seuntjens, P., Vanrolleghem, P.A., 2007. Monitoring and modeling pesticide fate in surface waters at the catchment scale. Ecol. Model. 209, 53–64. https://doi.org/10.1016/j.ecolmodel.2007.07.030.

Howard, A.D., Dietrich, W.E., Seidl, M.A., 1994. Modeling fluvial erosion on regional to continental scales. J. Geophys. Res. 99, 13971–13986. https://doi.org/10.1029/94JB00744.

Huber, E.R., Carlson, S.M., University of California, Berkeley, 2015. Temporal Trends in Hatchery Releases of Fall-Run Chinook Salmon in California's Central Valley. SFEWS 13. ⟨https://doi.org/10.15447/sfews.2015v13iss2art3⟩.

Jacobson, R.B., Galat, D.L., 2006. Flow and form in rehabilitation of large-river ecosystems: An example from the Lower Missouri River. Geomorphology 77, 249–269. https://doi.org/10.1016/j.geomorph.2006.01.014.
James, L.A., Singer, M.B., Ghoshal, S., Megison, M., 2009. Historical channel changes in the lower Yuba and Feather Rivers, California: Long-term effects of contrasting river-management strategies. In: Management and Restoration of Fluvial Systems with Broad Historical Changes and Human Impacts. Geological Society of America, Boulder, USA, pp. 57–81.
Johnson, B.W., McCulloch, R.E., 1987. Added – variable plots in linear regression. Technometrics 29, 427–433. https://doi.org/10.1080/00401706.1987.10488270.
Johnson, O.W., Grant, W.S., Kope, R.G., Neely, K.G., Waknitz, F.W., Waples, R.S., 1997. Status review of chum salmon from Washington, Oregon, and California (Technical Memorandum No. NMFS-NWFSC-32). National Marine Fisheries Service.
Jonsson, N., Jonsson, B., Hansen, L.P., 2003. The marine survival and growth of wild and hatchery-reared Atlantic salmon: Growth and survival of salmon. J. Appl. Ecol. 40, 900–911. https://doi.org/10.1046/j.1365-2664.2003.00851.x.
Kammel, L.E., Pasternack, G.B., Massa, D.A., Bratovich, P.M., 2016. Near-census ecohydraulics bioverification of (Oncorhynchus mykiss) spawning microhabitat preferences. J. Ecohydraul. 1, 62–78. https://doi.org/10.1080/24705357.2016.1237264.
Keefer, M.L., Caudill, C.C., 2014. Homing and straying by anadromous salmonids: a review of mechanisms and rates. Rev. Fish. Biol. Fish. 24, 333–368. https://doi.org/10.1007/s11160-013-9334-6.
Keefer, M.L., Clabough, T.S., Jepson, M.A., Johnson, E.L., Peery, C.A., Caudill, C.C., 2018. Thermal exposure of adult Chinook salmon and steelhead: Diverse behavioral strategies in a large and warming river system. PLoS ONE 13, e0204274. https://doi.org/10.1371/journal.pone.0204274.
Lamouroux, N., Souchon, Y., 2002. Simple predictions of instream habitat model outputs for fish habitat guilds in large streams: Habitat modelling for fish guilds. Freshw. Biol. 47, 1531–1542. https://doi.org/10.1046/j.1365-2427.2002.00880.x.
Larkin, P.A., 1979. Maybe you can't get there from here: a foreshortened history of research in relation to management of Pacific Salmon. J. Fish. Res. Bd. Can. 36, 98–106. https://doi.org/10.1139/f79-016.
Li, P., Zhang, W., Burnett, N.J., Zhu, D.Z., Casselman, M., Hinch, S.G., 2021. Evaluating dam water release strategies for migrating adult salmon using computational fluid dynamic modeling and biotelemetry. Water Res 57. https://doi.org/10.1029/2020WR028981.
Lupandin, A.I., 2005. Effect of flow turbulence on swimming speed of fish. Biol. Bull. Russ. Acad. Sci. 32, 461–466. https://doi.org/10.1007/s10525-005-0125-z.
MacFarland, T.W., Yates, J.M., 2016. Mann–Whitney U Test. Introduction to Nonparametric Statistics for the Biological Sciences Using R. Springer, Cham. ⟨https://doi.org/10.1007/978-3-319-30634-6_4⟩.
Marchetti, M.P., Moyle, P.B., 2001. Effects of flow regime on fish assemblages in a regulated California stream. Ecol. Appl. 11, 530–539. https://doi.org/10.1890/1051-0761(2001)011[0530:EOFROF]2.0.CO;2.
Massong, T.M., Montgomery, D.R., 2000. Influence of sediment supply, lithology, and wood debris on the distribution of bedrock and alluvial channels. Geol. Soc. Am. Bull. 112, 591–599. https://doi.org/10.1130/0016-7606(2000)112<591:IOSSLA>2.0.CO;2.
Maxwell, S., Gove, N., 2004. The feasibility of estimating migrating salmon passage rates in turbid rivers using a duel frequency identification sonar (DIDSON). Regional Information Report No. 2A04- 05. Alaska Department of Fish and Game, Anchorage, AK.
Maxwell, S.L., Gove, N.E., 2007. Assessing a dual-frequency identification sonars' fish-counting accuracy, precision, and turbid river range capability. J. Acoust. Soc. Am. 122, 3364–3377. https://doi.org/10.1121/1.2799500.
Mazerolle, M., 2020. Model Selection and Multimodel Inference Based on (Q)AIC(c) (Version 2.3–1), R Package. ⟨https://cran.r-project.org/package=AICcmodavg⟩.
McKnight, U.S., Rasmussen, J.J., Kronvang, B., Binning, P.J., Bjerg, P.L., 2015. Sources, occurrence and predicted aquatic impact of legacy and contemporary pesticides in streams. Environ. Pollut. 200, 64–76. https://doi.org/10.1016/j.envpol.2015.02.015.
Miller, J.P., 1958. High Mountain Streams: Effects of Geology on Channel Characteristics and Bed Material (Interpretation of quantitative measurements made in the Sangre de Cristo Range, north-central New Mexico No. Memoir 4). State Bureau of Mines and Mineral Resources and the New Mexico Institute of Mining and Technology. Socorro, New Mexico.
Moir, H.J., Pasternack, G.B., 2010. Substrate requirements of spawning Chinook salmon (*Oncorhynchus tshawytscha*) are dependent on local channel hydraulics: substrate requirements of spawning Chinook salmon. River Res. Appl. 26, 456–468. https://doi.org/10.1002/rra.1292.
Moir, H.J., Soulsby, C., Youngson, A.F., 2002. Hydraulic and sedimentary controls on the availability and use of Atlantic salmon (Salmo salar) spawning habitat in the River Dee system, north-east Scotland. Geomorphology 45, 291–308. https://doi.org/10.1016/S0169-555X(01)00160-X.
Moniz, P.J., Pasternack, G.B., Massa, D.A., Stearman, L.W., Bratovich, P.M., 2019. Do rearing salmonids predictably occupy physical microhabitat? J. Ecohydraul 1–19. https://doi.org/10.1080/24705357.2019.1696717.
Mora, E.A., Lindley, S.T., Erickson, D.L., Klimley, A.P., 2015. Estimating the riverine abundance of green sturgeon using a dual-frequency identification sonar. N. Am. J. Fish. Manag. 35, 557–566. https://doi.org/10.1080/02755947.2015.1017119.
Motulsky, H.J., Ransnas, L.A., 1987. Fitting curves to data using nonlinear regression: a practical and nonmathematical review. FASEB J. 1, 365–374. https://doi.org/10.1096/fasebj.1.5.3315805.
Moursund, R.A., Carlson, T.J., Peters, R.D., 2003. A fisheries application of a dual-frequency identification sonar acoustic camera. ICES J. Mar. Sci. 60, 678–683. https://doi.org/10.1016/S1054-3139(03)00036-5.
Mueller, A., Burwen, D.L., Boswell, K.M., Mulligan, T., 2010. Tail-beat patterns in dual-frequency identification sonar echograms and their potential use for species identification and bioenergetics studies. Trans. Am. Fish. Soc. 139, 900–910. https://doi.org/10.1577/T09-089.1.
Murdoch, A.R., Tonseth, M.A., Miller, T.L., 2009. Migration patterns and spawning distribution of adult hatchery sockeye salmon released as Parr from Net-Pens in Lake Wenatchee, Washington. N. Am. J. Fish. Manag. 29, 447–459. https://doi.org/10.1577/M08-051.1.
Nalin, R., Kotulla, M., 2018. Rapid Bedrock Incision by Water Stream Outburst: The Case of the Oroville Dam (California, USA). Geoscience Research Institute. URL https://www.grisda.org/rapid-bedrock-incision-by-water-stream-outburst-the-case-of-the-oroville-dam-california-usa-1 (accessed 2.26.21).
Nestler, J.M., Goodwin, R.A., Smith, D.L., Anderson, J.J., Li, S., 2008. Optimum fish passage and guidance designs are based in the hydrogeomorphology of natural rivers: natural hydrogeomorphology and fish passage design. River Res. Appl. 24, 148–168. https://doi.org/10.1002/rra.1056.
Nichols, A.L., Willis, A.D., Jeffres, C.A., Deas, M.L., 2014. Water temperature patterns below large groundwater springs: management implications for coho salmon in the Shasta River. Calif. River Res. Appl. 30, 442–455. https://doi.org/10.1002/rra.2655.
Nielsen, J.L., 1992. Microhabitat-specific foraging behavior, diet, and growth of Juvenile Coho Salmon. Trans. Am. Fish. Soc. 121, 617–634. https://doi.org/10.1577/1548-8659(1992)121%3C0617:MFBDAG%3E2.3.CO;2.
Olive, D.J., 2017. Multiple Linear Regression. In: Linear Regression. Springer International Publishing, Cham, pp. 17–83. ⟨https://doi.org/10.1007/978-3-319-55252-1_2⟩.
Ouellet, V., St-Hilaire, A., Dugdale, S.J., Hannah, D.M., Krause, S., Proulx-Ouellet, S., 2020. River temperature research and practice: Recent challenges and emerging opportunities for managing thermal habitat conditions in stream ecosystems. Sci. Total Environ. 736, 139679 https://doi.org/10.1016/j.scitotenv.2020.139679.
Penna, N., De Marchis, M., Canelas, O., Napoli, E., Cardoso, A., Gaudio, R., 2018. Effect of the junction angle on turbulent flow at a hydraulic confluence. Water 10, 469. https://doi.org/10.3390/w10040469.
Persinger, J.W., Orth, D.J., Averett, A.W., 2011. Using habitat guilds to develop habitat suitability criteria for a warmwater stream fish assemblage. River Res. Appl. 27, 956–966. https://doi.org/10.1002/rra.1400.
Peterson, M.L., Fuller, A.N., Demko, D., 2017. Environmental factors associated with the upstream migration of fall-run chinook salmon in a regulated river. N. Am. J. Fish. Manag. 37, 78–93. https://doi.org/10.1080/02755947.2016.1240120.
Peterson, D.A., Hilborn, R., Hauser, L., 2016. Exploratory behavior of dispersers within a metapopulation of sockeye salmon. BEHECO 27, 126–133. https://doi.org/10.1093/beheco/arv129.
Pipal, K.A., Notch, J.J., Hayes, S.A., Adams, P.B., 2012. Estimating escapement for a low-abundance steelhead population using dual-frequency identification sonar (DIDSON). N. Am. J. Fish. Manag. 32, 880–893. https://doi.org/10.1080/02755947.2012.697096.
Portet, S., 2020. A primer on model selection using the Akaike Information Criterion. Infect. Dis. Model. 5, 111–128. https://doi.org/10.1016/j.idm.2019.12.010.
Putman, N.F., Lohmann, K.J., Putman, E.M., Quinn, T.P., Klimley, A.P., Noakes, D.L.G., 2013. Evidence for geomagnetic imprinting as a homing mechanism in Pacific Salmon. Curr. Biol. 23, 312–316. https://doi.org/10.1016/j.cub.2012.12.041.
Quinn, T.P., 2018. The behavior and ecology of Pacific salmon and trout. In Association with American Fisheries Society, Second edition.,. University of Washington Press, Seattle: Bethesda, Maryland.
Quinn, T.P., Wetzel, L., Bishop, S., Overberg, K., Rogers, D.E., 2001. Influence of breeding habitat on bear predation and age at maturity and sexual dimorphism of sockeye salmon populations. Can. J. Zool. 79, 1782–1793. https://doi.org/10.1139/z01-134.
R Core Team, 2022a. R: A language and environment for statistical computing. R Foundation for Statistical Computing, Vienna, Austria (Rx64 Version 4.1.0).
R Core Team, 2022b. R Package: stats. (Version 3.6.2).
Rand, P.S., Hinch, S.G., Morrison, J., Foreman, M.G.G., MacNutt, M.J., Macdonald, J.S., Healey, M.C., Farrell, A.P., Higgs, D.A., 2006. Effects of river discharge, temperature, and future climates on energetics and mortality of adult migrating fraser river Sockeye Salmon. Trans. Am. Fish. Soc. 135, 655–667. https://doi.org/10.1577/T05-023.1.
Rheinheimer, D.E., Null, S.E., Lund, J.R., 2015. Optimizing selective withdrawal from reservoirs to manage downstream temperatures with climate warming. J. Water Resour. Plann. Manag. 141, 04014063.
Rice, S.P., 2017. Tributary connectivity, confluence aggradation and network biodiversity. Geomorphology 277, 6–16. https://doi.org/10.1016/j.geomorph.2016.03.027.
Richards, K.S., 1980. A note on changes in channel geometry at tributary junctions. Water Resour. Res. 16, 241–244. https://doi.org/10.1029/WR016i001p00241.
Ritz, C., Streibig, J.C., 2008. Nonlinear Regression with R, Use R! Springer, New York, NY.
Saltveit, S.J., Brabrand, Å., Brittain, J.E., 2019. Rivers need floods: Management lessons learnt from the regulation of the Norwegian salmon river, Suldalslågen. River Res Appl. rra 3536. https://doi.org/10.1002/rra.3536.
Schindler, D.E., Hilborn, R., Chasco, B., Boatright, C.P., Quinn, T.P., Rogers, L.A., Webster, M.S., 2010. Population diversity and the portfolio effect in an exploited species. Nature 465, 609–612. https://doi.org/10.1038/nature09060.
Shirvell, C.S., 1994. Effect of changes in streamflow on the microhabitat use and movements of sympatric Juvenile Coho Salmon (*Oncorhynchus kisutch*) and Chinook

Salmon (*O. tshawytscha*) in a Natural Stream. Can. J. Fish. Aquat. Sci. 51, 1644–1652. https://doi.org/10.1139/f94-165.

Silva, A.T., Katopodis, C., Santos, J.M., Ferreira, M.T., Pinheiro, A.N., 2012. Cyprinid swimming behaviour in response to turbulent flow. Ecol. Eng. 44, 314–328. https://doi.org/10.1016/j.ecoleng.2012.04.015.

Sklar, L.S., Dietrich, W.E., 2001. Sediment and rock strength controls on river incision into bedrock. Geology 29, 1087–1090. https://doi.org/10.1130/0091-7613(2001)029%3C1087:SARSCO%3E2.0.CO;2.

Sturrock, A.M., Satterthwaite, W.H., Cervantes-Yoshida, K.M., Huber, E.R., Sturrock, H.J. W., Nusslé, S., Carlson, S.M., 2019. Eight decades of hatchery salmon releases in the California central valley: factors influencing straying and resilience. Fisheries 44, 433–444. https://doi.org/10.1002/fsh.10267.

Tierney, K.B., Sampson, J.L., Ross, P.S., Sekela, M.A., Kennedy, C.J., 2008. Salmon olfaction is impaired by an environmentally realistic pesticide mixture. Environ. Sci. Technol. 42, 4996–5001. https://doi.org/10.1021/es800240u.

Tierney, K.B., Baldwin, D.H., Hara, T.J., Ross, P.S., Scholz, N.L., Kennedy, C.J., 2010. Olfactory toxicity in fishes. Aquat. Toxicol. 96, 2–26. https://doi.org/10.1016/j.aquatox.2009.09.019.

Tsuboi, J., Endou, S., Morita, K., 2010. Habitat fragmentation by damming threatens coexistence of stream-dwelling charr and salmon in the Fuji River, Japan. Hydrobiologia 650, 223–232. https://doi.org/10.1007/s10750-009-0076-3.

Weber, L.J., Goodwin, R.A., Li, S., Nestler, J.M., Anderson, J.J., 2006. Application of an Eulerian–Lagrangian–Agent method (ELAM) to rank alternative designs of a juvenile fish passage facility. J. Hydroinform. 8, 271–295. https://doi.org/10.2166/hydro.2006.006.

Wheaton, J.M., Bouwes, N., Mchugh, P., Saunders, C., Bangen, S., Bailey, P., Nahorniak, M., Wall, E., Jordan, C., 2018. Upscaling site-scale ecohydraulic models to inform salmonid population-level life cycle modeling and restoration actions - Lessons from the Columbia River Basin: Upscaling Ecohydraulic models. Earth Surf. Process. Landf. 43, 21–44. https://doi.org/10.1002/esp.4137.

Willis, J., 2011. Modelling swimming aquatic animals in hydrodynamic models. Ecol. Mod. 222, 3869–3887. https://doi.org/10.1016/j.ecolmodel.2011.10.004.